Version of Record: https://www.sciencedirect.com/science/article/pii/S0010218017303826
Manuscript_1d9c19cef2188851c03a33439e2c3d96

# Formulation of Optimal Surrogate Descriptions of Fuels Considering Sensitivities to Experimental Uncertainties

Pavan B. Govindaraju*,[a], Matthias Ihme[a]

[a] *Department of Mechanical Engineering, Stanford University, Stanford, CA, 94305, USA*

**Abstract**

Transportation fuels consist of a large number of species that belong to different families of compounds. Surrogate fuel representations have been formulated to better understand their fundamental chemical composition and to emulate combustion properties. These descriptions are formulated using experiments or through computations, which has thus led to the existence of two different notions of surrogates. There is further distinction of concepts through the use of physical and chemical surrogates, which are designed to emulate those specific properties. Although several surrogate design methodologies have been proposed in literature, they do not incorporate information on experimental uncertainty. By addressing this issue, it is shown that this information is crucial for the reliable construction of surrogates through computations. To incorporate physical fuel properties, a consistent approach through the use of the recent ASTM D2887 distillation curve standard is discussed. Then, a formal computational procedure is presented that incorporates information of experimental uncertainties into the surrogate description. It is shown that surrogates then describe a feasible region and are hence not unique. Both physical and chemical properties are utilized as combustion property targets (CPTs) and consistency with experimental formulations is demonstrated for JP-8 and Jet-A (POSF 4658) surrogates. In addition, the use of convex optimization puts existing concepts for surrogate representation on a more rigorous basis and several conclusions are drawn, particularly on the importance of specific CPTs and weighting factors of regression-based approaches. Also, the effect of using simplified models for the evaluation of CPTs on the final surrogate composition is shown by considering the example of linear blending rules for ignition delay. Finally, the surrogate representation problem is connected to multi-parametric optimization and bounds on surrogate compositions are calculated as a function of the experimental uncertainty along with comparisons against experimental results.

*Key words:* Surrogate fuel, Combustion property target, Parametric optimization, Sensitivity analysis, Uncertainty quantification

*Corresponding author
*Email addresses:* pavang@stanford.edu (Pavan B. Govindaraju), mihme@stanford.edu (Matthias Ihme)

# Technical Report Documentation Page

| 1. Report No. | 2. Government Accession No. | 3. Recipient's Catalog No. |
|---|---|---|
| j.combustflame.2017.09.044 | | |

| 4. Title and Subtitle | 5. Report Date |
|---|---|
| Formulation of optimal surrogate descriptions of fuels considering sensitivities to experimental uncertainties | November 2017 |
| | 6. Performing Organization Code |

| 7. Author(s) | 8. Performing Organization Report No. |
|---|---|
| Pavan B. Govindaraju, Matthias Ihme | |

| 9. Performing Organization Name and Address | 10. Work Unit No. (TRAIS) |
|---|---|
| Center of Excellence for: Alternative Jet Fuels and Environment<br><br>Stanford University, Department of Mechanical Engineering, Stanford, CA 94305, USA | 11. Contract or Grant No.<br><br>13-C-AJFE-SU-010 |

| 12. Sponsoring Agency Name and Address | 13. Type of Report and Period Covered |
|---|---|
| Federal Aviation Administration<br>Office of Environment and Energy | Journal Article |
| | 14. Sponsoring Agency Code |

15. Supplementary Notes

16. Abstract

Transportation fuels consist of a large number of species that belong to different families of compounds. Surrogate fuel representations have been formulated to better understand their fundamental chemical composition and to emulate combustion properties. These descriptions are formulated using experiments or through computations, which has thus led to the existence of two different notions of surrogates. There is further distinction of concepts through the use of physical and chemical surrogates, which are designed to emulate those specific properties. Although several surrogate design methodologies have been proposed in literature, they do not incorporate information on experimental uncertainty. By addressing this issue, it is shown that this information is crucial for the reliable construction of surrogates through computations. To incorporate physical fuel properties, a consistent approach through the use of the recent ASTM D2887 distillation curve standard is discussed. Then, a formal computational procedure is presented that incorporates information of experimental uncertainties into the surrogate description. It is shown that surrogates then describe a feasible region and are hence not unique. Both physical and chemical properties are utilized as combustion property targets (CPTs) and consistency with experimental formulations is demonstrated for JP-8 and Jet-A (POSF 4658) surrogates. In addition, the use of convex optimization puts existing concepts for surrogate representation on a more rigorous basis and several conclusions are drawn, particularly on the importance of specific CPTs and weighting factors of regression-based approaches. Also, the effect of using simplified models for the evaluation of CPTs on the final surrogate composition is shown by considering the example of linear blending rules for ignition delay. Finally, the surrogate representation problem is connected to multi-parametric optimization and bounds on surrogate compositions are calculated as a function of the experimental uncertainty along with comparisons against experimental results.

| 17. Key Words | 18. Distribution Statement |
|---|---|
| Surrogate fuel, Combustion property target, Parametric optimization, Sensitivity analysis, Uncertainty quantification, ASCENT |  |

| 19. Security Classif. (of this report) | 20. Security Classif. (of this page) | 21. No. of Pages | 22. Price |
|---|---|---|---|
| Unclassified | Unclassified | | |

**Contents**



## 1. Introduction

Transportation fuels consist of a large number of compounds that affect physical and chemical properties of the mixture. To simplify the complexity, these fuels are often represented by a surrogate description [1], which involves choosing a certain set of compounds, usually present in the original fuel, called *palette* compounds, to closely emulate certain properties of the present fuel. The significant challenge is, however, to determine the specific composition that best emulates relevant properties of interest while keeping the number of compounds small to reduce modeling complexity. The accepted quantities of interest are commonly referred to as combustion property targets (CPTs) [2]. These include both physical and chemical properties, namely density, viscosity, hydrogen-to-carbon ratio, aromaticity and cetane index [3]. Several surrogate studies have pursued these criteria based on empirical correlations or experimental testing [3, 4].

Pitz et al. [5, 6] reviewed efforts for gasoline and diesel fuels on surrogate formulations, kinetic model development, and experimental validation. Due to compositional variability of original fuels, it is important to choose combustion properties that capture the fuel description while being easy to measure and insensitive to procedural uncertainties. Dooley et al. [7] provided a list of CPTs in an aim to further develop a generic methodology for gas-phase combustion kinetic phenomena. Colket et al. [8] formulated a roadmap for the construction of jet fuel surrogates along with introducing and considering multiple surrogates for a particular fuel, depending on the CPTs.

Currently, two different paradigms of surrogates exist in the literature, namely experimental and computational surrogates. The former is the more widely adopted approach [7], which uses only experimental procedures to determine CPTs, from which surrogates are then determined. In contrast, the formulation of computational surrogates are a more recent approach and are determined by evaluating CPTs using only simulations. The accuracy of these so-defined computational surrogates in emulating the properties of the fuel dependents on computational models employed, and different modeling approaches can lead to different surrogate specifications; experimental confirmation of these surrogates is therefore necessary to ensure consistency. Reaction Design's *Surrogate Blend Optimizer* utilizes non-linear optimization algorithms to arrive at the surrogate mixture composition. This method was first described in [9] to construct a seven-component fuel blend for modeling gasoline. Several groups [10, 11, 12] utilize a computational approach by posing the determination of a surrogate composition as an optimization problem and utilizing both physical and chemical properties as CPTs. Aviation fuel surrogates have been derived using this approach of increasing palette sizes, with upto six-component surrogates being constructed [13]. However, common to all of these methods is the assumption of exact experimental fuel properties and a regression-based objective function that requires a weight for each CPT. This was improved upon more recently by Won et al. [14], by using experimental uncertainties to eliminate certain candidate mixtures formed as a result of discretization of the composition space. Each mixture is verified whether it indeed satisfies the constraints to the specified experimental thresholds, and is used to further narrow down the search space through a global search. Thus, there is a requirement for methods that incorporate and propagate experimental uncertainties to the final surrogate composition in a computationally efficient manner. This paper addresses this issue by providing a rigorous mathematical formulation for the surrogate representation problem along with methods to incorporate information on experimental uncertainty into the final surrogate description, which is shown to be necessary for reliable computational predictions.

Physical property emulation is another subject that requires more investigation in the area of surrogate representation. Violi et al. [3] matched volatility of fuels along with other chemical properties relevant for ignition using experimental techniques. Certain computational approaches for physical property emulation include matching only evaporation [15, 16] and distillation characteristics [17, 18, 19]. Ahmed et al. [11] utilized a computational approach for constructing surrogate compositions by including both physical and

chemical properties. However, the use of experimental distillation curves based on the ASTM D86 standard [20] and advanced distillation curve methodology (ADC) [21], as the descriptor of physical fuel characteristics is questionable due to experimental uncertainties of this approach. Recent advancements in the distillation standard [22] are shown in this paper to offer a solution which is consistent with a computational approach and to provide a viable characterization for distillation.

This paper primarily aims to quantify the effect of experimental uncertainty in the surrogate composition. The use of tools from optimization theory imparts rigor and helps quantifying bounds on compositions as a function of uncertainties. Certain experimental surrogate mixtures are utilized for benchmarks and provide a connection between the computational and experimental surrogate approaches.

Table 1 summarizes the palettes of various jet fuel surrogates used in this paper. The compounds present in these palettes are specifically chosen to be representative of different classes of organic compounds [2], which include n-paraffins, iso-paraffins, cycloparaffins and aromatic compounds. This variation also offers a suitable benchmark for CPT evaluations since a purely computational approach is adopted in this paper. Both 4- and 5-compound surrogates are used to highlight the palette size independence of the approach that will be developed in this paper. Note that the surrogate in Violi et al. [3] differs from both Stanford A and B mixtures [23] only in composition. However, the procedure described is shown to capture the necessary details and distinguish them even when the differences are not immediate. The surrogate due to Dooley et al. [7] relies on higher aromatics and serves as an important benchmark for both the chemical mechanism [24] and physical property evaluations, which is performed based on the group contribution method [25]. This surrogate also represents a different fuel (Jet-A POSF 4658) and is utilized to demonstrate that the procedure developed in the present work is independent of the underlying fuel description.

| Name | Methylcyclo-hexane | Tolu-ene | Ben-zene | iso-Octane | n-Dode-cane | n-Propylben-zene | 1,3,5-Trimethyl-benzene |
|---|---|---|---|---|---|---|---|
| Jet-A POSF 4658 (Dooley et al. [7]) | | | | 0.295 | 0.404 | 0.228 | 0.073 |
| JP-8 (Violi et al. [3]) | 0.1 | 0.1 | 0.01 | 0.055 | 0.735 | | |
| JP-8 (Stanford A [23]) | 0.1 | 0.1 | 0.01 | 0.25 | 0.54 | | |
| JP-8 (Stanford B [23]) | 0.1 | 0.295 | 0.01 | 0.055 | 0.54 | | |

Table 1: Abbreviated compounds used in palettes along with their mole fractions for jet fuel surrogates from [3, 7, 23], which are used for benchmarks in this paper.

The remainder of this paper is outlined as follows. The method used to incorporate physical properties and experimental uncertainties is described in detail in Section 2. First, a consistent approach to using distillation curves as a CPT is presented. Subsequently, the incorporation of experimental uncertainties in computational approaches to surrogate representations is discussed. The presented methodology is applied to the construction of jet fuel surrogates in Section 3, where limitations in current literature, such as the importance of a particular CPT and its connection to weighting factors in regression-based approaches is elaborated on. The effect of using simplified models for the CPT evaluation on the final surrogate composition is discussed in Section 3.3. A discussion on using more advanced optimization techniques to enable parametric studies on surrogates is presented in Section 4, along with relevant computational results. The paper finishes by summarizing the main contributions of this work and offering conclusions in Section 5.

## 2. Methodology

This section discusses in detail the methods aimed towards the problem of determining the surrogate composition under consideration of uncertainties that are introduced by experimental methods and computational models. After reviewing relevant CPTs in Section 2.1, Section 2.2 deals with the necessity of incorporating experimental uncertainties into the description of the surrogate composition. Then, Section 2.3 discusses methods that provide consistent descriptions of CPTs obtained through experiments and computations. The final subsection provides a detailed discussion of the surrogate representation problem under the framework of convex optimization and in turn, better quantifying the surrogate description of fuels.

### *2.1. Consistent description of CPTs*

To specify the surrogate composition from the palette of compounds, a set of CPTs [2, 7] are prescribed to constrain fundamental molecular properties that manifest in the occurrence of combustion-related phenomena. This approach has been used without specifically referring to them as CPTs in several previous studies [3, 8, 26]. CPTs can be broadly classified into physical and chemical target properties, with the former including molecular weight, H/C ratio and volatility, while ignition delay time (IDT) and threshold sooting index (TSI) are frequently used chemical target properties.

Consistent descriptions between experiments and computations are desired for CPTs to provide a unified representation of surrogates obtained using experimental and computational approaches. The various approaches used to evaluate commonly used CPTs is presented as follows [2]

- Molecular Weight: This property is directly evaluated using the composition; since it is a weighted average of individual molecular weights, this is a linear constraint on the mixture composition.
- H/C ratio: This constraint can also be evaluated directly from the composition and is also a linear constraint, since it can be recast into a set of linear inequations.

- Threshold Sooting Index: The TSI is experimentally based on the maximum smoke-free laminar diffusion flame height and can be predicted through a group-contribution approach [27]. Since this method only involves a linear combination of coefficients, TSI is a linear constraint for computational purposes.

- Ignition Delay Time: This is experimentally determined using a standardized ignition quality tester and the more relevant quantity of interest is the derived cetane number (DCN). DCN is expressed in non-dimensional units and varies inversely with the IDT [28]. The standard computational approach is to use a 0D-batch reactor simulation at specific conditions to evaluate this using a chemical mechanism. This mechanism is usually ensured to yield similar results between experiments and computations, but the margin of uncertainty is quite large. In the present work, the 451-species POLIMI mechanism is used to evaluate the ignition delay time from homogeneous ignition calculations [24, 29].

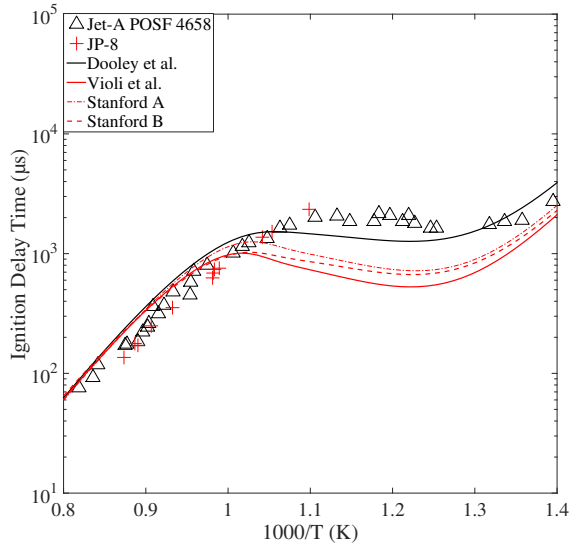


Figure 1: Comparison between experimental ignition delay time for Jet-A [2] and JP-8 measured in [23] at 20 atm and $\phi = 1$ with computations performed using the 451-species POLIMI mechanism [24, 29] for the surrogates listed in Table 1

Figure 1 presents the validation of the chemical mechanism against experimental data at 20 atm using a constant-volume batch reactor to calculate the auto-ignition delay time. Uncertainties in the shock tube measurements of around 15% [23] have been reported in the ignition delay time, but the computational predictions deviate to a larger extent and require incorporating a large error threshold to capture the experimental data. Thus, it is important that, given the current state of chemical mechanisms, a method to quantify uncertainty in surrogate descriptions must properly account for the specific error thresholds under consideration.

Other computational approaches to evaluating IDTs involve either pressure-based empirical corrections

[30], palette-specific regression models [14] or linear mixing rules [12] that hold true only at DCN conditions. Given the restrictions of these approaches and the additional interpolation error, which can be incurred in them, this work uses the entire POLIMI mechanism for obtaining the ignition delay times. This is computationally tractable as the ignition delay time can be evaluated in parallel and a computational ignition delay time calculator which leverages this parallelism has been developed and is utilized in this work (see Supplementary Information).

- Distillation Curve: The final CPT under consideration is the volatility of a fuel and is characterized using the distillation curve, which expresses the temperature as a function of the recovered mass fraction. This is usually obtained experimentally using the ASTM D86 standard [20]. Shortcomings of this procedure are discussed in detail by Bruno et al. [31], involving systematic errors that depend on apparatus geometry and heating rate. To isolate fuel effects from these measurements, uncertainty bounds for the distillation curve were provided in [25]. This involves determining both flash and fractional distillation limits, which represent either the limit of one or infinite vapor-liquid equilibrium interfaces, respectively. An experimental fractional distillation apparatus consists of a finite number of columns, with each corresponding to an equilibrium interface and hence, experimental results for fractional distillation can be bounded between the computational flash and fractional limits. The ASTM D2887 standard [22] improves upon previous standards by maintaining the same oven and injection temperatures, thus minimizing transient effects. Hence, the notion of determining the distillation curve was imprecise until date, but recent improvements to the experimental standard have been found to eliminate these systematic errors.

  Figure 2(a) shows that ASTM D2887 results closely follow the fractional distillation bounds predicted using computations. This is not the case using the ASTM D86 standard, as can be observed in Figure 2(a). The ASTM D2887 standard offers a precise notion of determining the distillation curve and a formalism to incorporate physical properties in the surrogate representation procedure. The area between the experimental data and computed fractional distillation curve, shaded in gray, is chosen as the objective function, which, in the limit of the palette compounds matching the full fuel description, tends to zero and thus offers a consistent description in representing physical properties.

  Figure 2(b) highlights the fact that the fractional approach to distillation is in better agreement with the D2887 standard as compared to the existing approach for evaluating distillation-curve as a CPT, which involve bubble-point calculations in steps of evaporated volume and is referred to as the 'step-volume' approach in this paper. This method was initially discussed in [32] in the context of surrogate fuel construction and later adopted in [12] for constructing surrogates emulating both physical and chemical properties of conventional jet fuels. Figure 2(b) shows a comparison between the fractional distillation curve, step-volume approach and the D2887 standard for two-surrogate

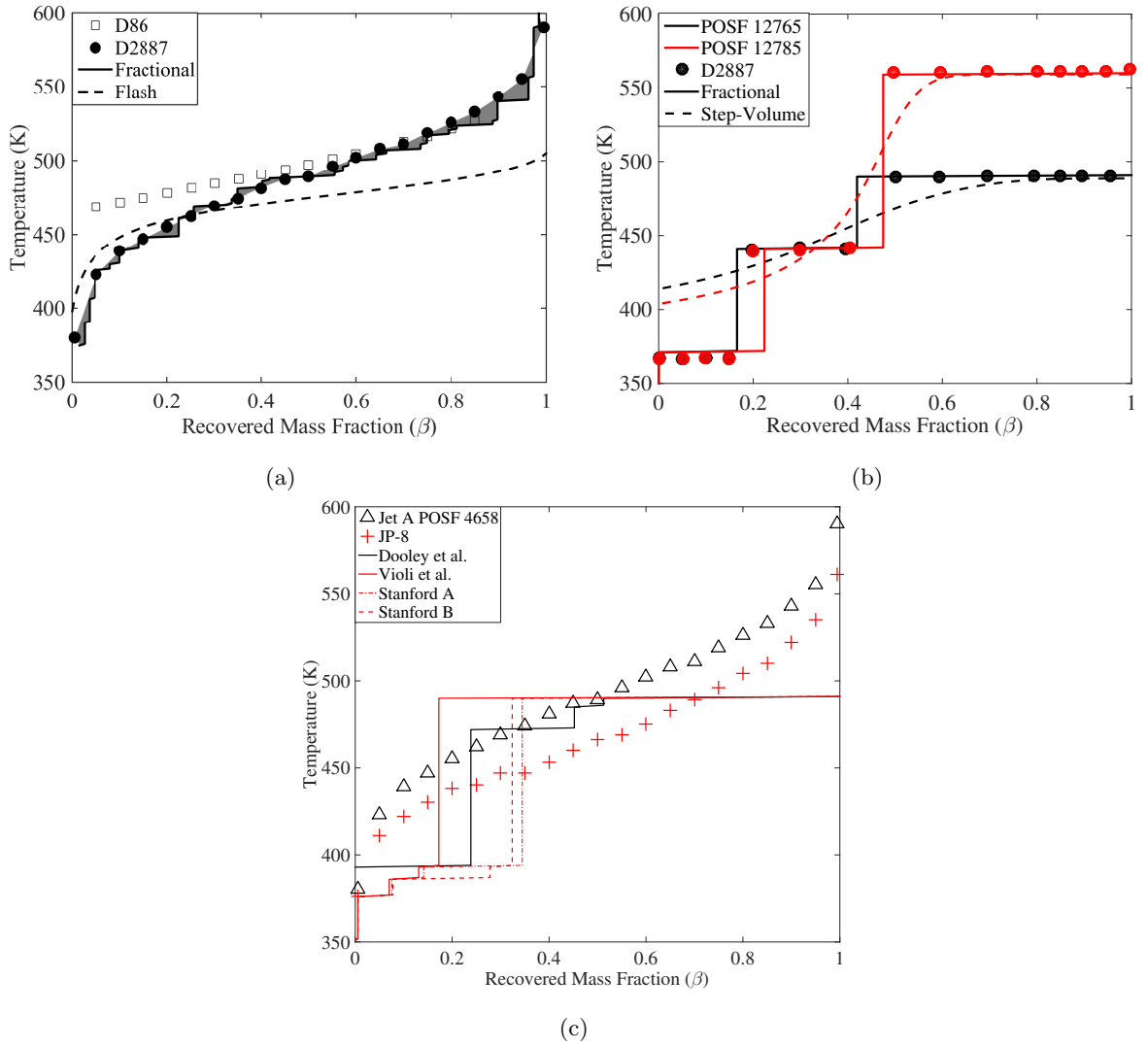


Figure 2: a) Distillation curve for POSF 4658 Jet-A experimentally measured using both D86 and D2887 standards. The flash and fractional bounds for the distillation curve are obtained using the procedure described in [25]. The area shaded in gray shows the difference between experimental D2887 curve and the computational fractional distillation b) Comparison between fractional distillation and step-volume approach [12, 32] against the experimental D2887 curve for Jet-A surrogates, POSF 12765 and POSF 12785 [33] c) Fractional distillation curve for surrogates listed in Table 1 along with D2887 distillation data for the corresponding full fuel descriptions from [33]

fuels, POSF 12765 and POSF 12785, which are two surrogates blended for the average Jet-A. These consist of 1,3,5-trimethylbenzene and iso-octane blended with either n-dodecane or n-hexadecane, thus closely resembling the palette for the POSF 4658 surrogate presented in Dooley et al. [7]. The fractional distillation approach captures both the length and height of the fractional distillation steps obtained using the ASTM D2887 standard. Although the step-volume approach was demonstrated to capture D86 standard distillation data for binary and ternary mixtures, the D2887 standard leads

to discontinuous distillation curves, which cannot be inherently captured using this method and thus, the fractional distillation method is advocated for eventual surrogate constructions.

The fractional distillation curves and associated objective functions are evaluated using the method described in [25] and is presented in Figure 2(c) for the surrogates listed in Table 1. The step profile of the distillation curve is indicative of the boiling temperature of each species and its proportion in the surrogate mixture. Using this method, all four surrogates distinguish themselves through this CPT, which is based only on physical properties.

### *2.2. Incorporating experimental uncertainties*

This subsection discusses the necessity of incorporating experimental uncertainties in the surrogate description of fuels. This is demonstrated through the variability due to ignition delay time errors in surrogate compositions. The ignition delay time is one of the combustion property targets used by Dooley et al. [7] and was introduced to account for the gas-phase kinetics of a fuel. Standard measurements for IDT involve uncertainties of the order of 15% [23], and reported experimental errors for DCN are less than unity [14]. Note that the ignition delay time obtained using computational techniques has a much larger uncertainty when compared with respect to the experimental data, and this has been highlighted in Figure 1. Most of all, the information on the error in CPTs has so far not been considered in existing methods to quantify uncertainties in surrogate composition. Ahmed et al. [11] presented an optimization procedure where weighting factors are assigned to each CPT and a global minimum for the objective function is evaluated, which corresponds to the final surrogate composition. The target property is assumed to be a fixed value and does not take into account the experimental uncertainty of the underlying CPT.

To assess the importance of this, simulations are performed, wherein the molecular weight and H/C ratio of the target fuel are matched exactly, similar to previous computational approaches [10] and then, the range of compositions corresponding to an IDT with at most 15% variation is evaluated. This is done for the surrogate presented in [3] and the Stanford A mixture in [23]. Note that this means three constraints are prescribed in the optimization problem, namely, molecular weight, H/C ratio and that the sum of mole fractions is unity. Thus, two degrees of freedom remain for a 5-compound palette and the range of compositions can now be depicted using a 2D plot. Other properties like TSI can also be included, but has not been chosen for this particular test case due to the fixed palette size and hence, the number of degrees of freedom.

The nomenclature adopted for the relevant equations is that both vectors and matrices are denoted in bold-face, with vectors in small letters and matrices in capitals, in accordance with standard notation in optimization. Given that the mole fractions of the palette composition, with number of species $N_s$, are denoted by $\mathbf{x} = [x_1, x_2, \ldots, x_{N_s}]^T$ and $\mathbf{m} = [m_1, m_2, \ldots, m_{N_s}]^T$ represents the molecular weights of each compound in the palette along with $\mathbf{h} = [n_{H,1}, n_{H,2}, \ldots, n_{H,N_s}]^T$ and $\mathbf{c} = [n_{C,1}, n_{C,2}, \ldots, n_{C,N_s}]^T$

representing the number of hydrogen and carbon atoms in each compound respectively, the feasibility region can be defined implicitly through a *feasibility problem*, or in other words, an optimization problem [11] with an irrelevant objective function, and hence assumed fixed. This feasibility problem can be formally written as

$$\begin{aligned} \underset{\mathbf{x}}{\text{minimize}} \quad & f(\mathbf{x}) = 1 \\ \text{subject to} \quad & \sum_{i=1}^{N_s} x_i = 1 \\ & \mathbf{m}^T\mathbf{x} = t_{MW} \\ & \frac{\mathbf{h}^T\mathbf{x}}{\mathbf{c}^T\mathbf{x}} = t_{HC} \end{aligned} \tag{1}$$

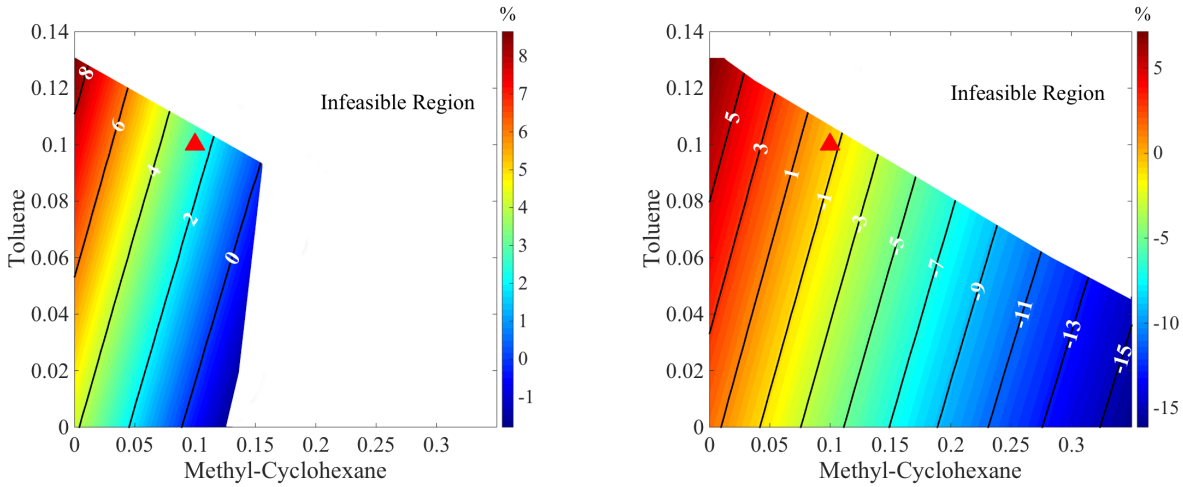


(a) JP-8 Surrogate from [3]

(b) JP-8 Surrogate from [23]

Figure 3: Contour plot of IDT deviation from experimental value at DCN conditions ($p_0$ = 22.4 bar and $T_0$ = 833 K) for surrogate compositions, which satisfy the respective given molecular weight and H/C ratio, as presented in [3] and Stanford A [23] for JP-8, also listed in Table 1. Note that the remaining components are not held constant but satisfy the constraints. The proposed experimental surrogate composition is marked by the red symbol

Figure 3 shows a map of the ignition delay times evaluated for the two surrogate compositions proposed in [3] and [23] for JP-8. Note that the three prescribed constraints are sufficient to narrow down the possible surrogate compositions to a set where the ignition delay times are indistinguishable within the experimental uncertainty of 15%. Even in the case of Figure 3(b), a major portion of the feasible region is indistinguishable and the prescribed constraints can be interpreted as leading to non-unique solutions to the surrogate optimization problem. This inspires an optimization formulation where constraints are not exact, but take into account uncertainties that are imposed from variations, among and between, experiments and computations.

*2.3. Convex optimization approach to surrogate representation*

This subsection presents formal procedures to incorporate experimental uncertainties into the description of surrogates through the use of tools from convex optimization. This procedure ensures convergence to the optimal, places no restrictions on the search space due to computational limitations and avoids the use of weighting factors. The error thresholds for CPTs serve as parameters for the optimization problem. The CPTs only specify constraints and thus, narrow down the search space for the surrogate composition. The key to efficiently incorporating uncertainty is through the use of an appropriate objective function and this section discusses how different objective functions can be used to provide concise descriptions of the search space.

Given that experimental uncertainties are described using tolerances centered at the reported value, a natural description of uncertainty in the surrogate composition would be through the use of a tolerance radius, centered at each mole fraction contained in the composition of a particular surrogate. The choice now lies between whether this range of compositions either *inscribes* or *circumscribes* the search space.

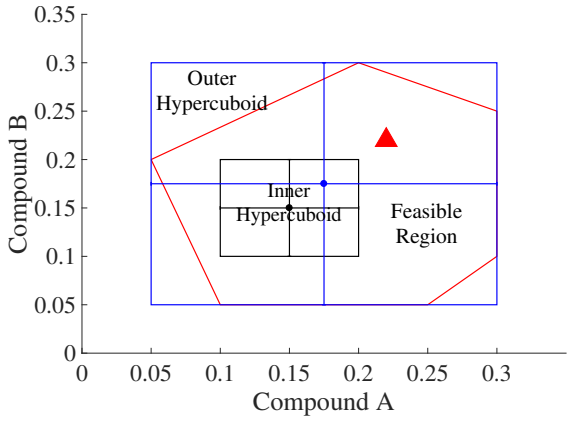


Figure 4: Illustration of the feasible region (in red) being inscribed (in black) and circumscribed (in blue) by hypercuboids

Figure 4 illustrates how the feasible region can be approximately described using inner and outer hypercuboids. The experimental composition, shown using the red triangle, need not necessarily lie within the inner hypercuboid, but must do so within the outer hypercuboid, as will be discussed in detail later in this section. The aim of characterizing the surrogate search space using this simplistic description is shown to also provide information regarding the importance of a particular compound in the palette and a measure of robustness for a particular surrogate description. Geometrically, a surrogate can be viewed as a point in a high-dimensional space, with the number of dimensions corresponding to the palette size. The problem of assigning tolerances to the surrogate composition corresponds to assigning a lower and upper bound for each palette compound. This can be viewed as finding an outer bounding box, or, more precisely, an outer bounding hypercuboid for the feasible region. Thus, outer tolerances represent the extreme limits of each

compound in the palette and that there is at least one feasible surrogate composition where these values are attained. Similarly, an inner bounding hypercuboid represents the largest tolerances that lie completely within the feasible region. This problem is tractable when the search space is a convex polytope and in the case of CPTs, which are linear, this is indeed the case. In case of nonlinear CPTs, examples of which include ignition delay time and error in distillation curve prediction, the convex hull based on feasible points can provide an accurate approximation to an arbitrary accuracy, if it is a convex constraint. For these particular properties, numerical evidence, shown in Figures 3 and 5, indicates that the sub-level sets, or in other words, regions with values less than a particular number, are indeed convex and hence the constraints themselves are convex [34, pg. 139]. Note that since each compound in the surrogate composition is characterized by a particular dimension, the desired hypercuboids must be aligned with the coordinate axes for the tolerances to correspond to compounds in the palette, which limits the accuracy of this description. However, if one is willing to carry the information of a transformation matrix instead of just tolerances, a more accurate description of the search space can be provided using other geometric objects and this will be discussed further in Section 2.3.2.

The constraints arising from CPTs on inclusion of experimental uncertainties become inequalities. Using the same notation as Eq. (1), the constraints can be summarized as

$$\begin{aligned} z(\mathbf{x};\epsilon_{MW},\epsilon_{HC},\epsilon_j) := \underset{\mathbf{x}}{\text{minimize}} \quad & f(\mathbf{x}) \\ \text{subject to} \quad & \sum_{i=1}^{N_s} x_i = 1 \\ & -\epsilon_{MW} \leq \mathbf{m}^T\mathbf{x} - t_{MW} \leq \epsilon_{MW} \\ & -\epsilon_{HC} \leq \frac{\mathbf{h}^T\mathbf{x}}{\mathbf{c}^T\mathbf{x}} - t_{HC} \leq \epsilon_{HC} \\ & F_j(\mathbf{x}) \in S_j(\epsilon_j) \qquad j = 1,2,\ldots,N_{nl} \end{aligned} \tag{2}$$

where $f$ stands for the objective function of choice, which is required to be a convex function. Appropriate choices for the objective function will be discussed in detail in Sections 2.3.1 and 2.3.2. Nonlinear CPTs, examples of which include the error norms on distillation curve or ignition delay time, are represented by $F_j(\mathbf{x})$. Also, $\epsilon_j$ represents the uncertainty for the $j^{th}$ nonlinear property target, which in turn determines the corresponding feasible region $S_j$, with $j = 1,2,\ldots,N_{nl}$, where $N_{nl}$ denotes the number of nonlinear constraints. Demarcating the region of interest can be simplified by evaluating the nonlinear constraint only in the feasible regions formed by the constraints in sequence. As an example, consider the problem for $\epsilon_{MW},\epsilon_{HC} = 0$, with the distillation curve error given by

$$\|T(\beta) - T_{exp}(\beta)\|_1 = \int_0^1 |T(\beta) - T_{exp}(\beta)|\ d\beta \tag{3}$$

Equation (3) serves as the sole nonlinear constraint in this illustrative example. This characterization of the distillation curve is appropriate as this CPT contains a series of measurements, or simply put, a

vector-valued function. Since a CPT error is required to be characterized by one scalar, a norm is chosen to map this vector to a scalar, and it is a well-known fact that discrete norms are equivalent to one another, thus making the choice of a particular norm irrelevant. Thus, the integral of the $\ell^1$-norm is chosen as it is intuitive and corresponds to the area between the experimental and computational distillation curves. The common approach to distillation curve error involves using only one temperature point, namely, the bubble point of the surrogate composition, is not advisable as the fuel vapor in practical settings is formed at various droplet temperatures as time proceeds and the whole curve is required to capture fuel behavior.

Given the distillation curves, the problem of evaluating the distillation curve error is equivalent to Eq. (1), but with one nonlinear constraint, namely, the error between computational and ASTM D2887 distillation curve. Thus, based on the suggestion for demarcating the region of interest, the ignition delay time only needs to be evaluated in the feasible region given by Eq. (1). This has been applied to the problem framed for the two surrogate compositions shown in Figure 3.

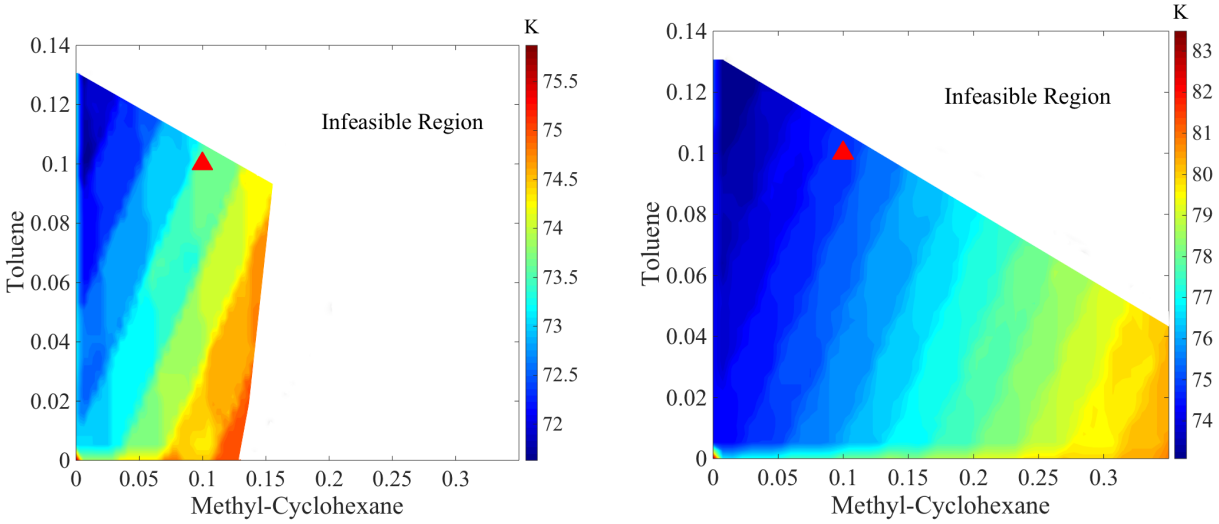


(a) JP-8 Surrogate from [3]

(b) JP-8 Surrogate from [23]

Figure 5: Contour plot of the $\ell^1$-norm for error between computational and ASTM D2887 distillation curve for surrogate compositions, which exactly satisfy ($\epsilon_{MW}, \epsilon_{HC} = 0$) the respective target molecular weight and H/C ratio for 2 of the 5 palette compounds, as presented in [3] and Stanford A mixture in [23] for JP-8. Note that the remaining components are not held constant but satisfy the constraints. The proposed experimental surrogate composition is marked by the red symbol

Note that the optimization problem has to be solved again whenever a different $\epsilon_j$ is utilized. However, if $\epsilon_{j,1} > \epsilon_{j,2}$, then the corresponding feasible spaces $S_{j,1}$ and $S_{j,2}$ are related by $S_{j,2} \subset S_{j,1}$, which essentially captures the fact that compositions within a certain tolerance also lie within a higher tolerance. Thus, a conservatively large value for $\epsilon_{j,1}$ could be chosen to determine the quantity of interest for an appropriately-sized search space so that the constraint function does not require repeated evaluation. This is especially useful when the constraint function evaluation is an expensive computation, which is definitely true in

the case of ignition delay time using large chemical mechanisms. The surrogate representation problem, presented in Eq. (2), can also be expressed in terms of relative errors using the simple transformation $\epsilon'_k = \epsilon_k / t_k$, for any constraint index $k$. This does not lead to any change in the approach used to solve the optimization problem as linearity is still preserved. The resulting problem is stated using relative tolerances as follows, and is the convention for the remainder of this paper.

$$
\begin{aligned}
z(\mathbf{x}; \epsilon'_{MW}, \epsilon'_{HC}, \epsilon'_j) := \underset{\mathbf{x}}{\text{minimize}} \quad & f(\mathbf{x}) \\
\text{subject to} \quad & \sum_{i=1}^{N_s} x_i = 1 \\
& t_{MW}(1 - \epsilon'_{MW}) \leq \mathbf{m}^T \mathbf{x} \leq t_{MW}(1 + \epsilon'_{MW}) \\
& t_{HC}(1 - \epsilon'_{HC}) \leq \frac{\mathbf{h}^T \mathbf{x}}{\mathbf{c}^T \mathbf{x}} \leq t_{HC}(1 + \epsilon'_{HC}) \\
& F_j(\mathbf{x}) \in S_j(\epsilon'_j)
\end{aligned}
\tag{4}
$$

Figure 5 shows a map of the error between computational and ASTM D2887 distillation curve for the two surrogate compositions proposed in [3] and [23] for JP-8, using the idea of reducing constraints in sequence before evaluating nonlinear constraints. It is important to note that the errors are high in magnitude, given that the surrogate composition distillation curve is based on at most five degrees of freedom in this case. The full composition is verified, in Figure 2a to give an error of less than 1 K for each of the distillation points. Note that the absolute magnitude of the distillation curve error is not relevant and in fact, depends on the temperature interval over which the distillation experiment is carried out. Also, the proposed experimental surrogate compositions clearly do not lie in the region of minimum error, which motivates the inclusion of physical properties in the surrogate description. It is useful to note that, since every constraint is being represented using convex polytopes, as justified in the beginning of this section, the search space can be concisely represented as $\mathbf{A}\mathbf{x} \leq \mathbf{b}$, for some $\mathbf{A}$ and $\mathbf{b}$, which only depend on the CPTs and the palette compounds. This is also evident in Figures 3 and 5, where the feasible region is given by polytopes. The objectives of the next sections are to give a concise description of surrogates along with error bounds. Two particular options are of interest, namely, representation using hypercuboids and hyperellipsoids.

### *2.3.1. Representation of search space using hypercuboids*

The representation of the surrogate formulation using a convex polytope is, however, not amenable to a concise description, which is required when reporting the composition of a surrogate. A more natural description, as presented in Section 2.2, is using a tolerance radius and this translates to bounds which are hypercuboids in composition space. Once the constraints from CPTs have been represented as a convex polytope, the problem of finding the inner and outer hypercuboids can be written as a convex optimization problem. This is where an appropriate objective function has to be utilized and details regarding the

optimization problem and its numerics are presented in Appendix A.1.

As an example for illustrative purposes, only the linear constraints, namely molecular weight and H/C ratio, from Eq. (4) are used on the Jet-A POSF 4658 surrogate given by Dooley et al. [7]. Note that TSI is also a linear constraint and is used later in this work. The relative error thresholds have been set to 0.05 for molecular weight, which corresponds to around 6g/mol, and 0.005 in the case of H/C ratio, as its average value is around 2 and a variation of 0.01 is reported [14].

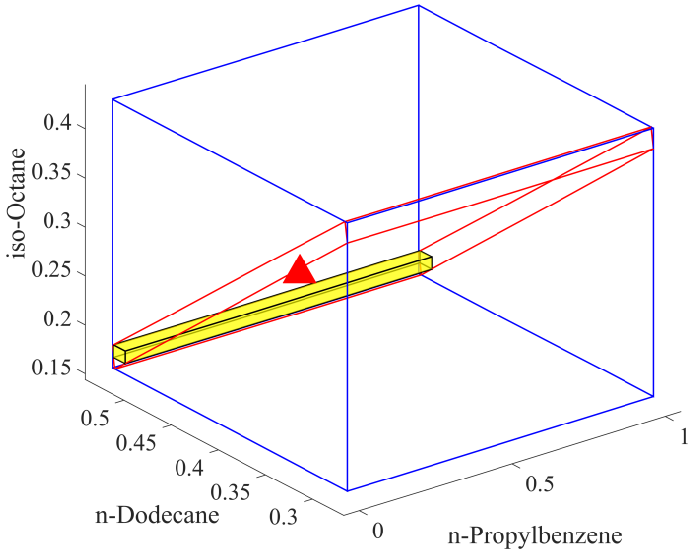


Figure 6: Feasible region (in red outline) from linear constraints in Eq. (4) along with inner (in yellow) and outer (in blue outline) hypercuboids for the 4-compound Jet-A surrogate in [7] corresponding to the three degrees of freedom for mole fractions. The error thresholds for molecular weight $\epsilon'_{MW} = 0.05$ and $\epsilon'_{HC} = 0.005$ based on uncertainties reported in [14]. The red triangle depicts the proposed experimental composition

Figure 6 provides a visualization in composition space of the various constraints imposed in the optimization procedure. Note that the surrogate depictions involve one dimension less than the number of palette compounds as the mole fraction of the final compound is enforced using the sum constraint. Thus, a 3D visualization is possible in the case of this surrogate mixture as the palette consists of four compounds. Larger palette sizes must be visualized using projections, preferably pairwise and hence, in two dimensions. The polyhedron in Figure 6 corresponds to the feasible region demarcated by the molecular weight and H/C ratio constraints. The inner (in yellow) and outer hypercuboid (in blue outline) are obtained from the solution of a series of optimization problems presented in Appendix A.1.

A physical interpretation of these characterizations is that the inner hypercuboid represents a sufficient estimate of the uncertainty, in that, every composition within it definitely satisfies the CPTs. Note that the corresponding experimental surrogate compositions need not be contained in this region. The outer hypercuboid is more conservative and can be interpreted as a necessary estimate of the uncertainties, or in

other words, compositions satisfying all the constraints must at least lie within the outer hypercuboid. The fact that both inner and outer hypercuboid are required for containing the experimental composition is to be noted as it can lie outside the inner hypercuboid but must lie within the outer hypercuboid, given that it satisfies the constraints. In addition, the experimental composition lying within the feasible region obtained using computations is deemed as a 'consistent' surrogate as there are both experimental and computational results predicting a composition that satisfies the CPTs. This is trivial in the case of CPTs that can be evaluated in the form of linear constraints like molecular weight and H/C ratio, but would serve as a benchmark when other nonlinear constraints are included, as will be shown in Section 3.

Other geometrical objects that also result from solutions of convex optimization problems can be used for describing the search space and are discussed in the next section.

#### *2.3.2. Representation of search space using hyperellipsoids*

The tolerances could alternatively be interpreted as the semi-axis lengths of hyperellipsoids thus leading to the question of whether a hyperellipsoid would make a better descriptor of the search space. Hyperellipsoids can be described as images of unit hyperspheres, given by $\|\mathbf{w}\|_2 \leq 1$, under invertible linear transformations $\mathbf{Bw} + \mathbf{x}$; in symbolic form, a particular hyperellipsoid $\mathcal{E}$ can be represented as [34, pg. 30]

$$\mathcal{E} = \{\mathbf{Bw} + \mathbf{x} \text{ such that } \|\mathbf{w}\|_2 \leq 1\} \tag{5}$$

Note that $\mathbf{B}$ can be assumed, without loss of generality, to be a positive-definite matrix, as it results only from the stretching and rotation of the principal axes. Further details regarding the bounding ellipsoids and their construction are presented in Appendix A.2. The problem of constructing hyperellipsoids not just involves a different objective function, but is numerically distinct from the construction of hypercuboids, as it is an example of a *semi-definite program* (SDP), where the constraints involve semi-definite variables. These problems require specific solvers [35, 36]. However, this additional effort leads to better approximations of the search space as it at least captures the axis-aligned hyperellipsoid if it is indeed the maximum-volume case. However, the search space must now be described using not just the center of the ellipsoid, or in other words, the candidate composition $\mathbf{x}$, but also the transformation matrix $\mathbf{B}$. The axis-aligned hyperellipsoid does not require this additional matrix for its description and can also be obtained using a more straightforward optimization problem; the details of which are presented in Appendix A.2. Note that the same approach used for axis-aligned hyperellipsoids can be used for the more general case of an arbitrary convex geometric object. The largest scaling factor can be calculated such that it can be embedded entirely within the search space using optimization techniques. This is more commonly referred to as the *diamond cutting problem* [37] and it is important to distinguish it from the problems discussed in this section as the aspect ratio and orientation are fixed by the prescription of the object.

To illustrate the ellipsoid calculations, the axis-aligned and maximum volume hyperellipsoid are constructed for the Jet-A surrogate in [7] using only molecular weight and H/C ratio. The visualizations have been generated using the *Ellipsoidal Toolbox* for MATLAB [38].

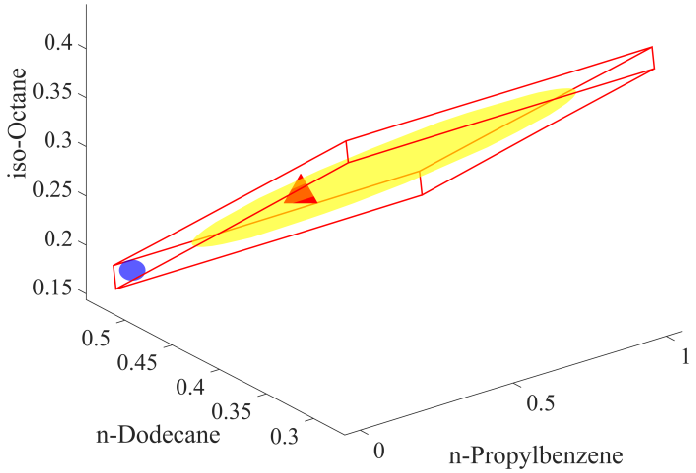


Figure 7: Feasible region (in red outline) from linear constraints in Eq. (4) along with axis-aligned (in blue) and maximum-volume (in yellow) hyperellipsoids for the 4-compound Jet-A surrogate in [7] corresponding to the three degrees of freedom for mole fractions. The error thresholds for molecular weight $\epsilon'_{MW} = 0.05$ and $\epsilon'_{HC} = 0.005$ based on uncertainties reported in [14]. The red triangle depicts the proposed experimental composition

Figure 7 depicts the axis-aligned (in blue) and maximum-volume hyperellipsoid (in yellow), along with the experimental composition. Note that alignment with the axes severely restricts the proportion of the feasible region which is captured. The maximum-volume hyperellipsoid contains the experimental composition within itself and is true even for the feasible region (in red outline). Thus, consistency between experimental and surrogate compositions is noted even when hyperellipsoids are used to characterize this mixture. The orientation of the maximum-volume ellipsoid with respect to the coordinate axes is evident and allows to capture a larger volume of the feasible region.

## 3. Applications

This section utilizes the methods described in Section 2 to construct and verify surrogate compositions using both physical and chemical properties. This primarily involves extending the usage to non-linear constraints, which is done by constructing a map of the non-linear function in the feasible region and approximating its boundary using a convex hull. It is obvious that one could come up with a nonlinear function which leads to feasible regions that are non-convex sets. The present study deals with ignition delay time and the error norm of the distillation curve, which are shown through numerical evidence, already presented in Figures 3 and 5, to be representable using convex sets and thus form the sole non-linear constraints for the subject of this discussion. The information of experimental uncertainty is incorporated

into candidate surrogate compositions and is summarized as tolerances for proposed mole fractions. The section concludes with a discussion on the importance of particular CPTs and their relation to weighting factors in regression-based approaches for surrogate representations [10, 11].

It is important to remember that two distinct notions of surrogates exist in literature, namely experimental and computational surrogates, which are based on disconnected approaches. The former involves evaluating CPTs only using experimental approaches, while the latter predominantly utilizes computational models of varying fidelity to evaluate them and particularly, for the step to determine the optimal surrogate composition. The primary contribution of this study and also the focus of this section, is to ensure a consistent description of these notions of surrogates by providing bounds for surrogate compositions that are determined through computations and verifying if the experimental composition also lies within these limits. This geometrically corresponds to the experimental surrogate composition to be required to lie in the interior of the hypercuboids or hyperellipsoids determined using the computational approach. Examining this aspect is the subject of discussion in the following subsection.

### *3.1. Error tolerances of sample surrogate*

The full optimization problem includes the use of TSI calculated using a mixture-averaged rule as a linear group-contribution approach [27], which was shown to be successful in predicting experimental values. The pure-compound TSI values are written as $\boldsymbol{\theta} = [\theta_1, \theta_2, \ldots, \theta_{N_s}]^T$. In addition, two nonlinear properties, namely ignition delay time and the distillation curve error, defined in Section 2.3, are also utilized. The ignition delay times are first evaluated over a discrete set of surrogate compositions, with a resolution of 50 points along each dimension of the surrogate composition vector in the outer hypercuboid region using the reduction discussed in Section 2.3. This amounts to around 50,000 test compositions for the four mixtures listed in Table 1, whose ignition delay time is to be evaluated using the full mechanism. The ignition delay time computations were performed in parallel using 768 processors and required under five hours. The convex hull of the resultant points is constructed and forms the feasible region of interest. The objective function $f$ is selected based on the geometric object (details of which are provided in Appendix A) used to describe the points in the feasible region. This is chosen to be the volume for both inner hypercuboids and maximal-volume hyperellipsoids. The outer hypercuboid is constructed using the coordinates in each dimension as the objective function to be either minimized or maximized. Axis-aligned hypercuboids are constructed by obtaining the maximum scaling factor. Details regarding the numerics are also presented in

Appendix A. The full optimization problem can be summarized as

$$
\begin{aligned}
z(\mathbf{x};\epsilon'_{MW},\epsilon'_{HC},\epsilon'_{TSI},\epsilon'_{IDT},\epsilon'_{DC}) := \quad & \min_{\mathbf{x}} && f(\mathbf{x}) \\
& \text{subject to} && \sum_{i=1}^{N_s} x_i = 1 \\
& t_{MW}(1-\epsilon'_{MW}) && \leq \mathbf{m}^T\mathbf{x} \leq t_{MW}(1+\epsilon'_{MW}) \\
& t_{HC}(1-\epsilon'_{HC}) && \leq \frac{\mathbf{h}^T\mathbf{x}}{\mathbf{c}^T\mathbf{x}} \leq t_{HC}(1+\epsilon'_{HC}) \\
& t_{TSI}(1-\epsilon'_{TSI}) && \leq \boldsymbol{\theta}^T\mathbf{x} \leq t_{TSI}(1+\epsilon'_{TSI}) \\
t_{DC}(1- \quad & \epsilon'_{DC}) \leq \|T(\beta) - T_{exp}(\beta)\|_1 \leq t_{DC}(1+\epsilon'_{DC}) \\
t_{IDT}(1- \quad & \epsilon'_{IDT}) \leq \tau_{IDT_{comp}}(\mathbf{x};p_0,T_0,\phi) \leq t_{IDT}(1+\epsilon'_{IDT})
\end{aligned}
\tag{6}
$$

The error thresholds have been chosen based on experimental uncertainties presented in literature. Won et al. [14] report conservative estimates for uncertainties of various CPTs. The distillation curve error is calculated based on the fact that the error observed in [14] is around 1 K. Also, noting that the average values of distillation curve error shown in Figure 5, is around 80 K, a value of $\epsilon'_{DC} = 0.0125$ is utilized. Other thresholds used in this section are summarized in the following table

| CPT | Average Value | Experimental Error | Threshold |
|---|---|---|---|
| Molecular Weight | 120 (g/mol) | 6 (g/mol) | 0.05 |
| H/C Ratio | 2 | 0.01 | 0.005 |
| Threshold Sooting Index | 25 | 1 | 0.04 |
| Ignition Delay | 50 | 1 | 0.02 |
| Distillation Curve Error | 80 (K) | 1 (K) | 0.0125 |

Table 2: Relative error thresholds used for quantifying uncertainty in surrogate descriptions based on experimental uncertainties reported in Won et al. [14]

Note that the prescribed error thresholds are bound to change with improvements in experimental techniques and this paper primarily demonstrates the method of uncertainty quantification, which does not explicitly depend on the error thresholds.

The ignition delay time, which varies inversely with DCN is chosen as a constraint because the correlations used for converting to DCN are fuel-dependent, and to isolate its effect from the uncertainty evaluation. For the same reason, simulations of the ignition delay time are performed at DCN conditions and they correspond to a stoichiometric mixture undergoing ignition at $p_0 = 22.4$ bar and $T_0 = 833$ K. It is noted that the current method enables the consideration of different target conditions and combustion properties.

The computational ignition delay time at the experimental composition was chosen as the representative $t_{IDT}$ for comparison as this offers a fair benchmark and does not include mechanism errors in it, given

that both comparative and representative values are calculated using the same chemical mechanism. This is clearly seen in Figure 1, where a large error, of up to an order of magnitude, is required to encompass the experimental ignition delay times while centered at the computationally predicted values, especially in the predicted negative temperature coefficient (NTC) region. Thus, the ignition delay time at the experimental surrogate composition is being used for calibrating computational ignition delay times. This can be equally performed with any other composition and thus allows for usage of this method even in situations where there is no available information on the surrogate apart from the list of compounds in the palette. This step is essential when the underlying computational models cannot match the experimental values as the specified target of a real fuel might not be achievable using any composition. Alternatively, one might suggest that the computational composition which provides the closest approximation to the target be utilized. This alternative approach is not applicable when multiple CPTs do not have a consistent description as the compositions which best approximate for one property need not do so for another, thus not leading to a feasible solution. Also, information on uncertainty cannot be utilized as the composition which best approximates is usually a single composition because the problem then simplifies to finding the maximum or minimum CPT in the feasible region, depending on whether the target exceeds or is lower than all possible computational values for the CPT.

Since the primary focus of this study is the characterization of sensitivities, it is necessary to use consistent measurements given the strong dependence of ignition delay time on the method of measurement. In any case, this paper presents a generalized approach to this characterization and the method as such, remains robust irrespective of the procedure used to evaluate constraints. The objective function is chosen based on the geometric object under consideration, as described in detail in Appendix A.

The distillation curve error norm is obtained using the computed fractional distillation curve and the full fuel measurement based on the D2887 standard. This was already verified in Section 2.1 to provide a consistent basis for a constraint estimate and thus enables a physical CPT evaluation for any candidate composition. This is essential for computational surrogate characterizations as every optimization procedure requires the ability to evaluate constraints for any proposed composition. The target value for the distillation curve error is chosen to be the value obtained on performing the calculation using the experimental surrogate composition.

The first application uses the surrogate mixture described in [7] for Jet-A using four compounds. Note that projections have been used to present this surrogate as well even though a 3D representation, similar to Figures 6 and 7, depicts all degrees of freedom. Information regarding the experimental composition being present in the interior of the calculated regions is crucial to determining the consistency of a surrogate and this can be decisively conveyed only through 2D images on paper. Both hypercuboid and hyperellipsoid characterizations are presented for completeness and is repeated for all surrogates listed in Table 1.

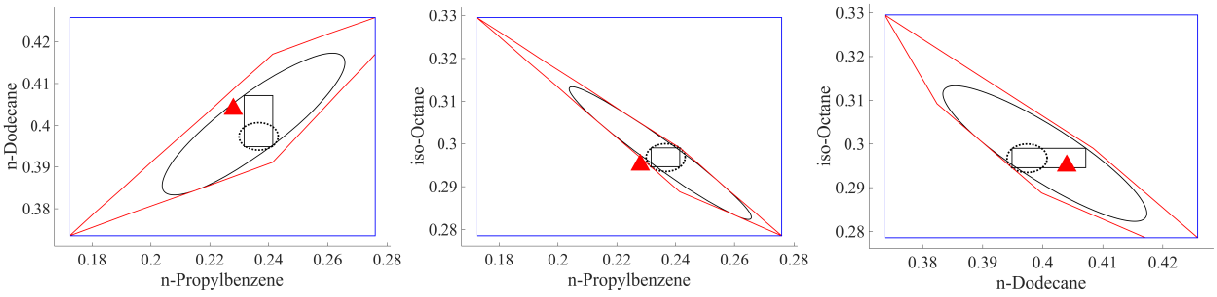


Figure 8: Projections in 2D of the feasible region in Eq. (6) (in red), inner and outer hypercuboids (in blue), along with axis-aligned ( . . . . . ) and maximum-volume (————) hyperellipsoids for the 4-compound Jet-A surrogate in [7], also listed in Table 1. The relative error thresholds are summarized in Table 2. The red triangle depicts the proposed experimental composition

Figure 8 presents various characterizations for the 4-compound Jet-A surrogate [7]. It is important to remember that the area of the feasible region in the projection can be vastly larger compared to the size of a cross-section. However, all inscribed and circumscribed geometrical objects remain similarly confined also in the projections. The minimal requirement for a consistent surrogate description between experiments and computations is that the experimental surrogate composition lies completely within the feasible region (in red). Figure 8 shows that the experimental composition is within the feasible region even when the D2887-based distillation curve error, an example of a CPT that was not considered during experiments, is utilized as well. The inner hypercuboid and axis-aligned hyperellipsoid present a rigid estimate of the error threshold in composition space, and it would be the hallmark of an experimental surrogate to lie completely within those prescribed computational bounds. Note that the maximal-volume hyperellipsoid is the most successful in capturing the shape and volume of the feasible region, but requires additional information regarding axes orientation. Also, the outer hypercuboid demarcates extremes in mole fractions and is a better representation of the feasible region, especially in the case where its range is narrow in a particular dimension and the inscribed geometrical figures occupy only a small fraction of the feasible region, for instance, the projection onto iso-octane and n-propylbenzene axes.

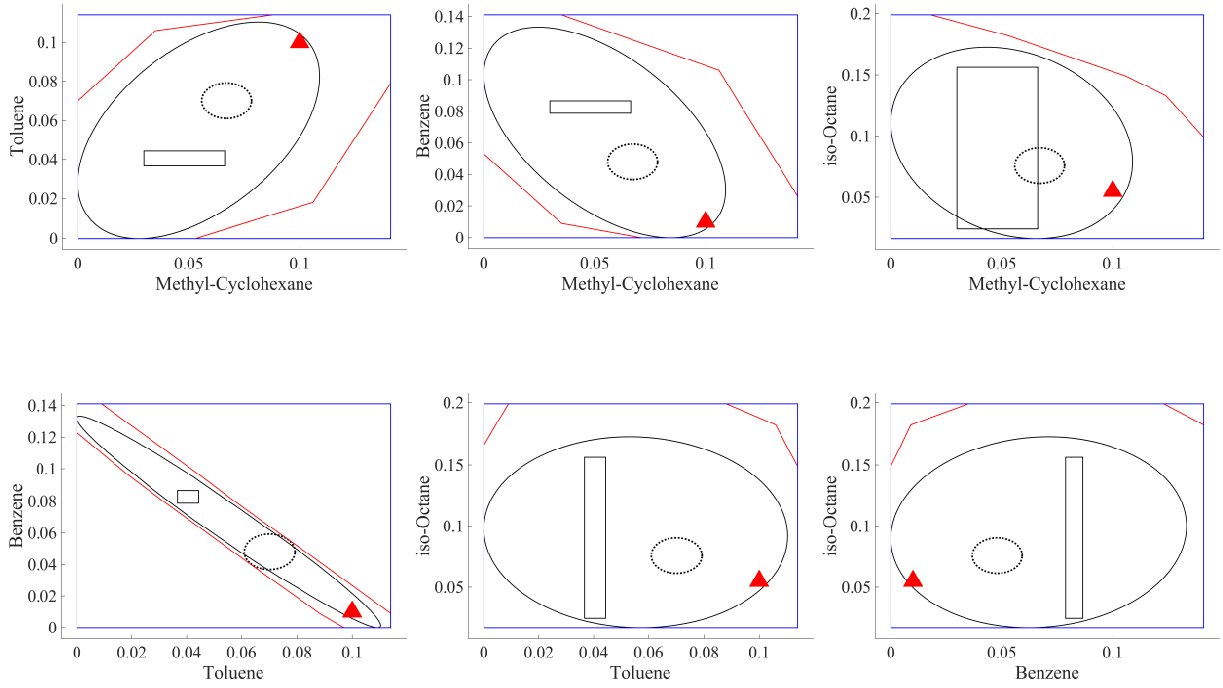


Figure 9: Projections in 2D of the feasible region in Eq. (6) (in red), inner and outer hypercuboids (in blue), along with axis-aligned (. . . . . ) and maximum-volume (————) hyperellipsoids for the 5-compound JP-8 surrogate in [3], also listed in Table 1. The relative error thresholds are summarized in Table 2. The red triangle depicts the proposed experimental composition

Figure 9 shows the results for the JP-8 surrogate presented in [3] and illustrates the method for a different fuel. There is agreement between experimental and computational surrogate descriptions as the experimental composition always lies within the feasible region (in red) demarcated by CPTs and in fact, within the maximal volume hyperellipsoid. The number of projections increases as there are now five compounds in the palette and in fact, the number of projections given the palette size $N_s$ is equal to $(N_s - 1)(N_s - 2)/2$. Note that the inner hypercuboid and hyperellipsoid is primarily restricted by Benzene and Toluene. Also, the inner geometric objects provide rigid limits to the composition given the uncertainty and are well within the interior of the feasible region.

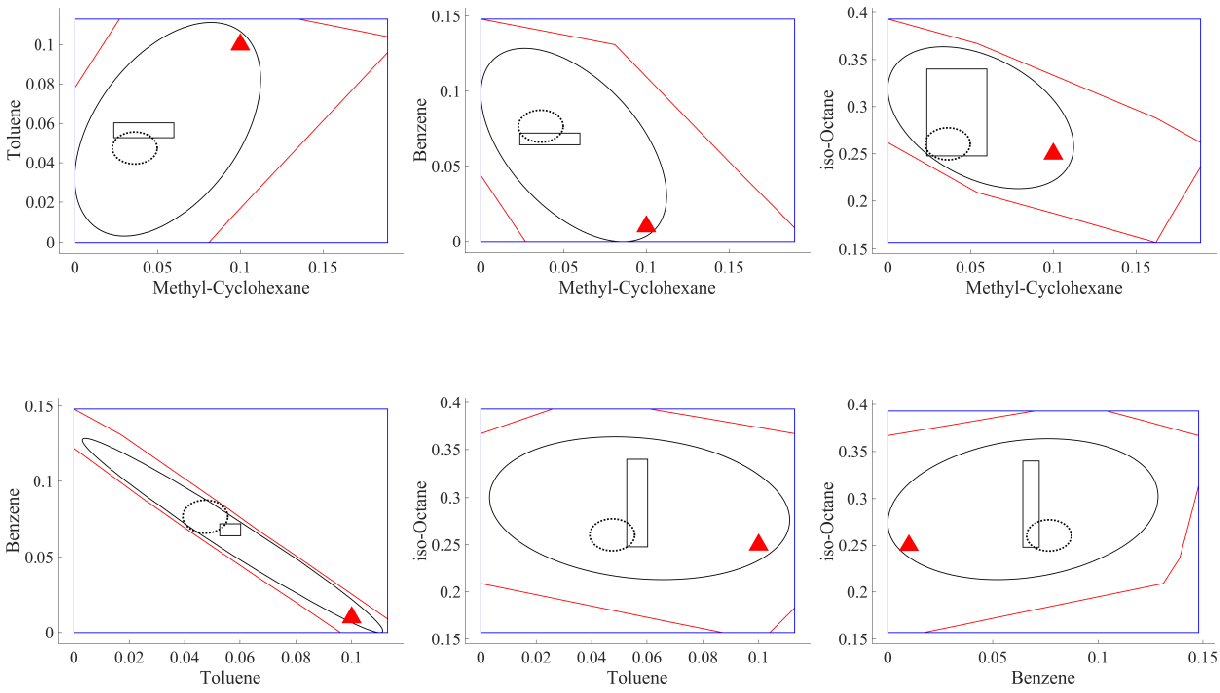


Figure 10: Projections in 2D of the feasible region in Eq. (6) (in red), inner and outer hypercuboids (in blue), along with axis-aligned (. . . . . ) and maximum-volume (————) hyperellipsoids for the 5-compound JP-8 surrogate (Stanford A) in [23], also listed in Table 1. The relative error thresholds are summarized in Table 2. The red triangle depicts the proposed experimental composition

The JP-8 surrogates presented in [23] form the remaining part of the discussion in this subsection. Figure 10 shows that there is agreement with the experimental and computational surrogate descriptions as the experimental composition always lies within the feasible region demarcated by CPTs. Also, the maximal volume hyperellipsoid captures the experimental composition. Similar to the JP-8 surrogate of [3], the inner hypercuboid and hyperellipsoid are primarily restricted by Benzene and Toluene.

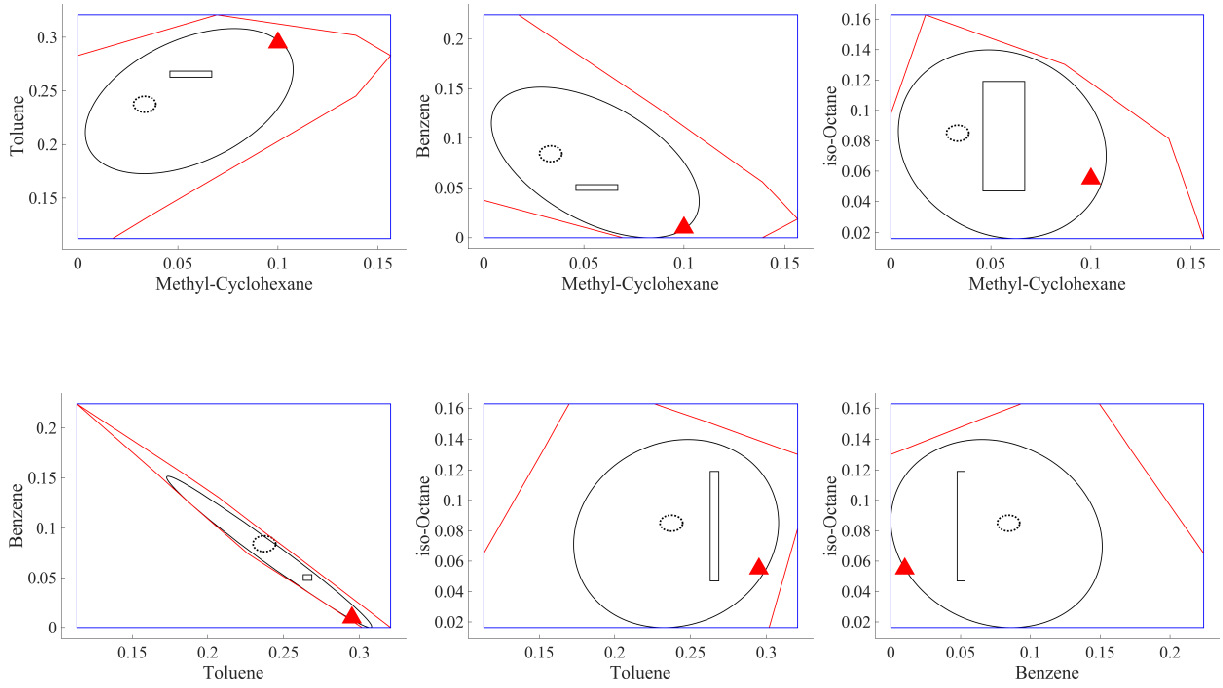


Figure 11: Projections in 2D of the feasible region in Eq. (6) (in red), inner and outer hypercuboids (in blue), along with axis-aligned (. . . . . ) and maximum-volume (————) hyperellipsoids for the 5-compound JP-8 surrogate (Stanford B) in [23], also listed in Table 1. The relative error thresholds are summarized in Table 2. The red triangle depicts the proposed experimental composition

Figure 11 further confirms that the method developed in this work distinguishes surrogates with the same palette compounds but with slightly different compositions, as can be seen by comparing Figures 10 and 11. The bottleneck for the inner geometric description is once again evident in the Benzene-Toluene pair.

An important advantage of using hypercuboids to describe the surrogate composition is that another candidate can be readily evaluated to be lying within the inner hypercuboid region by just checking the individual coordinates. This is not the case with the hyperellipsoid, where one has to evaluate $(\mathbf{x}' - \mathbf{x})^T(\mathbf{B}\mathbf{B}^T)^{-1}(\mathbf{x}' - \mathbf{x}) \leq 1$ to verify if the composition $\mathbf{x}'$ indeed lies within a hyperellipsoid centered at $\mathbf{x}$ and the eigenvalues of $\mathbf{Q} = \mathbf{B}\mathbf{B}^T$ yield the principal axes lengths. The maximum-volume ellipsoid has an accompanying full matrix for $\mathbf{Q}$, which needs to be provided as part of the surrogate description and can be cumbersome. However, this is a trade-off in favor of higher packing fractions of the search space and consistent capturing of the proposed experimental compositions is a decision to be made based on requirements.

In summary, the surrogate descriptions for the four candidate fuel mixtures is presented along with the bounds based on error thresholds in Table 2. Thus, all four surrogate descriptions presented in Table 1 can be deemed as consistent given the CPTs under consideration, which include both physical and chemical

properties. The consistent nature of the surrogates under consideration is quite a coincidence because different methodologies have been used to obtain the CPTs and also, the property targets differed between the experimental studies. It also motivates the question of importance of a particular CPT, since the addition of certain CPTs has not violated the existing surrogate descriptions. This question is certainly of importance and is discussed in detail in the next section.

| Name | Compound | Experiment | Inner Hypercuboid | Outer Hypercuboid |
|---|---|---|---|---|
| Dooley et al. [7] | n-Propylbenzene | 0.228 | 0.236 ± 0.004 | 0.224 ± 0.051 |
| | n-Dodecane | 0.404 | 0.401 ± 0.006 | 0.399 ± 0.026 |
| | iso-Octane | 0.295 | 0.296 ± 0.002 | 0.304 ± 0.025 |
| | Trimethylbenzene | 0.073 | (*) | (*) |
| Violi et al. [3] | Methylcyclohexane | 0.1 | 0.047 ± 0.018 | 0.070 ± 0.070 |
| | Toluene | 0.1 | 0.040 ± 0.003 | 0.057 ± 0.057 |
| | Benzene | 0.01 | 0.082 ± 0.004 | 0.070 ± 0.070 |
| | iso-Octane | 0.090 | 0.090 ± 0.065 | 0.108 ± 0.091 |
| | n-Dodecane | 0.735 | (*) | (*) |
| Stanford A [23] | Methylcyclohexane | 0.1 | 0.041 ± 0.018 | 0.094 ± 0.094 |
| | Toluene | 0.1 | 0.056 ± 0.003 | 0.056 ± 0.056 |
| | Benzene | 0.01 | 0.068 ± 0.003 | 0.074 ± 0.074 |
| | iso-Octane | 0.25 | 0.293 ± 0.046 | 0.275 ± 0.118 |
| | n-Dodecane | 0.54 | (*) | (*) |
| Stanford B [23] | Methylcyclohexane | 0.1 | 0.056 ± 0.010 | 0.078 ± 0.078 |
| | Toluene | 0.295 | 0.265 ± 0.002 | 0.216 ± 0.103 |
| | Benzene | 0.01 | 0.050 ± 0.002 | 0.112 ± 0.112 |
| | iso-Octane | 0.055 | 0.083 ± 0.036 | 0.089 ± 0.073 |
| | n-Dodecane | 0.54 | (*) | (*) |

Table 3: Summary of experimental surrogate composition and its hypercuboidal characterization using error thresholds presented in Table 2 for molecular weight, H/C ratio, TSI, distillation curve error and ignition delay time at DCN conditions for the jet fuel surrogates proposed in [3, 7, 23]. The last species is obtained from enforcing total species conservation and is denoted by (*)

Tables 3 and 4 provide a summary of results obtained for the four surrogate mixtures considered here; $\mathbf{x}_{AA}$ and $\mathbf{x}_{MV}$ denote the centers of axis-aligned and maximum-volume hyperellipsoid, respectively. The calculated centers of all inscribed objects, or in other words, the surrogate compositions corresponding to the centers of the inner hypercuboid, axis-aligned hyperellipsoid and maximum-volume hyperellipsoid are indeed verified to satisfy the target properties. This is a direct consequence of the construction procedure

| Name | Compound | $\mathbf{x}_{AA}$ | $\mathbf{x}_{MV}$ | Transformation Matrix ($\mathbf{Q}^{1/2}$) |
|---|---|---|---|---|
| Dooley et al. [7] | n-propylbenzene | 0.236 ± 0.006 | 0.234 | $\begin{bmatrix} 0.027 & 0.009 & -0.011 \\ & 0.012 & -0.005 \\ & & 0.009 \end{bmatrix}$ |
| | n-Dodecane | 0.397 ± 0.003 | 0.400 | |
| | iso-Octane | 0.296 ± 0.003 | 0.297 | |
| | Trimethylbenzene | (*) | (*) | |
| Violi et al. [3] | Methylcyclohexane | 0.067 ± 0.011 | 0.058 | $\begin{bmatrix} 0.050 & 0.010 & -0.015 & -0.006 \\ & 0.039 & -0.037 & -0.000 \\ & & 0.053 & 0.001 \\ & & & 0.077 \end{bmatrix}$ |
| | Toluene | 0.070 ± 0.009 | 0.055 | |
| | Benzene | 0.047 ± 0.011 | 0.066 | |
| | iso-Octane | 0.075 ± 0.014 | 0.094 | |
| | n-Dodecane | (*) | (*) | |
| Stanford A [23] | Methylcyclohexane | 0.036 ± 0.013 | 0.056 | $\begin{bmatrix} 0.051 & 0.009 & -0.014 & -0.012 \\ & 0.038 & -0.036 & -0.003 \\ & & 0.050 & 0.004 \\ & & & 0.073 \end{bmatrix}$ |
| | Toluene | 0.047 ± 0.008 | 0.057 | |
| | Benzene | 0.076 ± 0.010 | 0.064 | |
| | iso-Octane | 0.260 ± 0.016 | 0.288 | |
| | n-Dodecane | (*) | (*) | |
| Stanford B [23] | Methylcyclohexane | 0.033 ± 0.005 | 0.055 | $\begin{bmatrix} 0.048 & 0.008 & -0.015 & -0.004 \\ & 0.048 & -0.045 & 0.002 \\ & & 0.057 & -0.005 \\ & & & 0.061 \end{bmatrix}$ |
| | Toluene | 0.237 ± 0.007 | 0.240 | |
| | Benzene | 0.084 ± 0.008 | 0.075 | |
| | iso-Octane | 0.084 ± 0.005 | 0.078 | |
| | n-Dodecane | (*) | (*) | |

Table 4: Summary of hyperellipsoidal characterizations using error thresholds presented in Table 2 for the jet fuel surrogates proposed in [3, 7, 23]. $\mathbf{x}_{AA}$ and $\mathbf{x}_{MV}$ correspond to axis-aligned (AA) and maximum-volume (MV) centers respectively. The last species is obtained from enforcing total species conservation and is denoted by (*)

as the center lies in the feasible region, given that the geometric objects are inscribed within it. Further details regarding the verification of computational surrogates is presented in Appendix B.

In the context of numerics, it is important to note that the transformation matrix is always symmetric, given that it is obtained by solving a semi-definite program, presented in Eq. (14), where it is required that $\mathbf{B}$ is positive-definite. The ellipsoid matrix $\mathbf{Q}$, as previously described in this section, is given by $\mathbf{B}\mathbf{B}^T$. Since $\mathbf{B}$ is symmetric (positive-definite), it follows that $\mathbf{B}$ can be equally represented using $\mathbf{Q}^{1/2}$ as the Cholesky decomposition $\mathbf{Q} = \mathbf{B}\mathbf{B}^T$ is unique for symmetric matrices.

The runtime to generate the table of results is of the order of a few seconds, given the ignition delay time maps, which are obtained as discussed in Section 2.3. The IDT maps are generated for a larger threshold (than 0.02 in this case) so that the optimization routines for a different threshold can be repeated without

additional overhead. The following sections discuss the utility of this approach in providing information regarding the importance of a particular CPT and its connection to weighting factors.

### *3.2. Importance of particular CPTs*

Previous computational approaches [10, 11] framed the problem of surrogate representation using a scalar objective function despite it being a vector optimization problem, where errors between multiple properties need to be minimized. This is a standard technique in optimization theory and is called *scalarization*, which is used to find the *Pareto optimal* of a given vector optimization problem. The problem of surrogate representation falls under the specific category of *multicriterion optimization*, where the components of the vector objective are comprised of scalar functions $F_i(\mathbf{x})$ corresponding to the constraints.

It is useful to define that a point $\mathbf{x}$ is 'better' than $\mathbf{y}$ if $F_i(\mathbf{x}) \leq F_i(\mathbf{y})$ for all $i$, as it simplifies the concept of a *Pareto optimal* point, which is defined as a point for which no other feasible point is better than it. Thus, there can be a set of points called the *Pareto surface*, which solely consist of Pareto optimal points. When this surface is just one point, it is called the *optimal* and coincides with the notion of *optimal* for a vector optimization problem. Further details regarding these concepts are well-described and illustrated in [34, pg. 174-180]. One important result is that any arbitrary positive weighting factor will result in a Pareto-optimal for the surrogate representation problem if the final scalar problem can be exactly solved. The design of appropriate weighting factors is necessary only to carefully explore the Pareto surface. It is important to remember that these weighting factors are exactly the essence of *duality* and the remainder of this section will provide a more formal basis for existing techniques to determine importance factors through this connection.

The objective function of the regression model used in [10, 11] is precisely the *Lagrangian dual function* of the optimization problem in Eq. (6), with error thresholds set exactly to zero, since the experimental properties are assumed to be exact. The weighting factors are the *dual variables* associated with the original, or in other words, *primal* problem. The Lagrange dual function only gives a lower bound on the optimal of the primal problem. A natural question is then to find the optimal weighting factors so that the best lower bound is obtained. Thus, the problem of determining the most appropriate weighting factors is equivalent to solving the *dual* problem for Eq. (6). The difference between the optimal for the primal and dual problem is referred to as the *duality gap* and this is zero only under special conditions, which are referred to as *constraint qualifications*. Several results regarding this exist in the literature and are discussed in detail for nonlinear constraints in [39]. Thus, claims of optimal computational surrogate compositions arrived using the weighting factor approach, even in the ideal situation of having the best weighting factors, must be made only when constraint qualification can be rigorously proved for each of the CPTs. Adding to the list of shortcomings for existing computational approaches [10, 11] is whether the scalar non-linear optimization approach used indeed finds the global optimal, given the complicated nature of the constraints

imposed by CPTs and the coarse-grained approach to finding weighting factors, both of which are issues acknowledged by the authors. These issues are avoided in this work by connecting optimal dual variables to weighting factors.

When both the objective function and constraints are convex, a simple condition exists for constraint qualification and is commonly referred to as *Slater's condition* [34, pg. 226]. This serves as one of the main reasons for adhering to a convex reformulation in the current approach, in addition to the provability of convergence for various numerical methods used to solve the optimization problem. Slater's condition simply states that if the problem is convex and there exists a point which is *strictly feasible*, or in other words, every inequality in Eq. (6) is strictly satisfied, then the duality gap is zero. This holds trivially as the condition is violated only if all points are feasible but not in the strict sense. In such a situation, the error threshold can be infinitesimally perturbed as it is an input parameter and the points are now strictly feasible. Thus, a scalar optimization approach can indeed be used to solve the problem in Eq. (6) and the resultant surrogate composition is indeed the optimal, assuming the convex reformulation is performed using a large enough map of the nonlinear constraints.

The definition for importance factors provided in [11] depends on how the weighting factors are increased, which has been done in powers of 10 to span a global range. Along with it, for a particular set of CPTs, the weighting factor is dependent on the particular optimization process, which should not be the case. Under conditions of strong duality, this notion can be made more consistent. For a constraint $F_i(\mathbf{x}) \leq v_i$, let $p^*(\mathbf{v})$ denote the optimal value of the objective function for a given $\mathbf{v}$ and that the original problem is defined to be when $\mathbf{v} = \mathbf{0}$. The optimal dual variables $\boldsymbol{\lambda}^*$, which are identical to the weighting factors under strong duality, are in fact linked to the objective function and constraints through the result [34, pg. 249].

$$-\frac{\partial p^*}{\partial v_i}(0) = \lambda_i^* \tag{7}$$

The left-hand-side quantity in Eq. (7) is referred to as the *sensitivity coefficient* of a particular constraint. This can be written specifically for Eq. (6) and thus, the sensitivity coefficient of each CPT, denoted by $\gamma_i$, is defined as

$$\gamma_j = -\frac{1}{t_j}\frac{\partial f}{\partial \epsilon'_j} \tag{8}$$

where $f$ corresponds to the objective functions used in Section 2.3 and $t_j$ is the target value of the $j^{\text{th}}$ CPT. However, only the inner hypercuboid and maximum-volume ellipsoid can be utilized for this purpose. This is because the problem of finding the outer hypercuboid involves solution to multiple optimization problems and as this involves several objective functions, a consistent definition of sensitivity coefficient cannot be made. Similarly, the axis-aligned hyperellipsoid involves objective functions in a coordinate system which

is stretched as a function of the error thresholds themselves and the objective function will thus not reveal the exact sensitivity to the thresholds.

It is important to remember that the sensitivity coefficient $\gamma_i$ between different objective functions cannot be compared. Even in the case of comparing different CPTs using the same objective function, one must not ascribe meaning to the absolute number, but only to the relative magnitudes of the sensitivity coefficients, since the objective function is unrelated to any CPT as it is based on a measure of the feasible region. It is for this reason that sensitivity coefficients defined using this method are recommended to be reported as a unit vector. As an example, the weighting factors are calculated by solving the dual problem, which is automatically performed by the optimization solver, using only linear constraints as discussed in Section 2.3, for the purpose of maintaining strong duality.

| Name | Inner Hypercuboid | | MV Hyperellipsoid | |
|---|---|---|---|---|
| | $\gamma_{MW}$ | $\gamma_{HC}$ | $\gamma_{MW}$ | $\gamma_{HC}$ |
| Dooley et al. [7] | 0.0 | 1.0 | 0.044 | 0.999 |
| Violi et al. [3] | 0.0 | 1.0 | 0.0 | 1.0 |
| Stanford A [23] | 1.0 | 0.0 | 0.044 | 0.999 |
| Stanford B [23] | 1.0 | 0.0 | 0.044 | 0.999 |

Table 5: Sensitivity coefficients for Eq. (6) when characterized using the inner hypercuboid along and maximum-volume (MV) hyperellipsoid at error thresholds for molecular weight ($\gamma_{MW}$) and H/C ratio ($\gamma_{HC}$) presented in Table 2. Values have been rounded to zero if less than $10^{-6}$

Table 5 provides a summary of the sensitivity coefficients at the same error thresholds of $\epsilon_i'$ used to generate the results in Section 3.1 for molecular weight and H/C ratio. The results illustrate that the importance of a CPT is specific to the objective function, especially in the case of the surrogate mixtures in [23], where, depending on whether the inner hypercuboid or maximum-volume hyperellipsoid is used to characterize the search space, the sensitivity coefficients are modified. Thus, optimal weighting factors and in this case, sensitivity coefficients, should not be used as a measure of importance for CPTs in general as they are dependent on the objective function. They only help to quantify whether a particular constraint is active, or in other words, provides a characterization of the importance of a particular CPT for that optimal. Also, what is more practically relevant is the sensitivity of the mole fraction of a particular compound to the change in error threshold. For this, one must be able to solve the optimization problem itself as a function of the error threshold. This motivates an approach where the error threshold is also a parameter and this is the subject of discussion for Section 4.

### *3.3. Effect of CPT models*

The use of palette-specific regression models or linear blending rules has been commented upon in Section 2.1, but the effect of using such schemes on the final surrogate composition remains to be probed. This subsection discusses the results obtained by swapping the ignition delay time using the full mechanism with a linear blending rule for DCN. Kim et al. [12] use a volume-fraction weighted approach for obtaining the DCN of candidate mixtures. Ahmed et al. [11] construct surrogates using a linear blending rule for the research octane number (RON), with mole fraction being suggested as an alternative. This blending rule has been used in this study for a fair comparison. The surrogate constructed using the linear blending rule was compared in [11] with the mixture calculated using batch reactor simulations and controlled autoignition CO profiles in an engine were measured for these fuels. The linear blending rule based fuel was found to consistently exhibit higher reactivity of around 10%, thus highlighting the deviation due to simplified models for CPTs. Also, multiple blending models developed for the purpose of octane number prediction in fuel blends require a non-linear correction term and it is a well-acknowledged fact that linear blending rules cannot predict the octane number in numerous situations [40].

The optimization problem described in Eq. (6) is solved with the IDT constraint replaced by a DCN constraint and the error threshold being the same as prescribed for IDT in Table 2. The DCN is obtained using a linear mole-fraction blending rule [11], written as $DCN = \mathbf{d}^T\mathbf{x}$, where $\mathbf{d} = [d_1, d_2, \ldots, \mathrm{d}_{N_s}]$ represents the pure-component DCNs, which has been obtained from [41].

| Name | Compound | Inner Hypercuboid | Blended Inner Hypercuboid | Outer Hypercuboid | Blended Outer Hypercuboid |
|---|---|---|---|---|---|
| Dooley et al. [7] | n-Propylbenzene | 0.236 ± 0.004 | 0.245 ± 0.004 | 0.224 ± 0.051 | 0.258 ± 0.017 |
| | n-Dodecane | 0.401 ± 0.006 | 0.406 ± 0.004 | 0.399 ± 0.026 | 0.404 ± 0.013 |
| | iso-Octane | 0.296 ± 0.002 | 0.291 ± 0.002 | 0.304 ± 0.025 | 0.288 ± 0.010 |
| | Trimethylbenzene | (*) | (*) | (*) | (*) |
| Violi et al. [3] | Methylcyclohexane | 0.047 ± 0.018 | 0.040 ± 0.006 | 0.070 ± 0.070 | 0.070 ± 0.070 |
| | Toluene | 0.040 ± 0.003 | 0.034 ± 0.004 | 0.057 ± 0.057 | 0.057 ± 0.057 |
| | Benzene | 0.082 ± 0.004 | 0.095 ± 0.004 | 0.070 ± 0.070 | 0.070 ± 0.070 |
| | iso-Octane | 0.090 ± 0.065 | 0.104 ± 0.006 | 0.108 ± 0.091 | 0.091 ± 0.074 |
| | n-Dodecane | (*) | (*) | (*) | (*) |
| Stanford A [23] | Methylcyclohexane | 0.041 ± 0.018 | 0.070 ± 0.005 | 0.094 ± 0.094 | 0.067 ± 0.067 |
| | Toluene | 0.056 ± 0.003 | 0.051 ± 0.003 | 0.056 ± 0.056 | 0.061 ± 0.052 |
| | Benzene | 0.068 ± 0.003 | 0.066 ± 0.003 | 0.074 ± 0.074 | 0.069 ± 0.069 |
| | iso-Octane | 0.293 ± 0.046 | 0.281 ± 0.004 | 0.275 ± 0.118 | 0.274 ± 0.065 |
| | n-Dodecane | (*) | (*) | (*) | (*) |
| Stanford B [23] | Methylcyclohexane | 0.056 ± 0.010 | 0.050 ± 0.004 | 0.078 ± 0.078 | 0.086 ± 0.069 |
| | Toluene | 0.265 ± 0.002 | 0.224 ± 0.002 | 0.216 ± 0.103 | 0.235 ± 0.066 |
| | Benzene | 0.050 ± 0.002 | 0.090 ± 0.003 | 0.112 ± 0.112 | 0.074 ± 0.074 |
| | iso-Octane | 0.083 ± 0.036 | 0.107 ± 0.004 | 0.089 ± 0.073 | 0.081 ± 0.065 |
| | n-Dodecane | (*) | (*) | (*) | (*) |

Table 6: Summary of hypercuboidal characterization using error thresholds presented in Table 2 with IDT or linear mole-fraction blended DCN for the jet fuel surrogates proposed in [3, 7, 23]. The last species is obtained from enforcing total species conservation and is denoted by (*)

| Name | Compound | $\mathbf{x}_{AA}$ | Blended $\mathbf{x}_{AA}$ | $\mathbf{x}_{MV}$ | Blended $\mathbf{x}_{MV}$ |
|---|---|---|---|---|---|
| Dooley et al. [7] | n-Propylbenzene | 0.236 ± 0.006 | 0.247 ± 0.006 | 0.234 | 0.250 |
| | n-Dodecane | 0.397 ± 0.003 | 0.404 ± 0.004 | 0.400 | 0.407 |
| | iso-Octane | 0.296 ± 0.003 | 0.290 ± 0.003 | 0.297 | 0.290 |
| | Trimethylbenzene | (*) | (*) | (*) | (*) |
| Violi et al. [3] | Methylcyclohexane | 0.067 ± 0.011 | 0.052 ± 0.009 | 0.058 | 0.058 |
| | Toluene | 0.070 ± 0.009 | 0.056 ± 0.007 | 0.055 | 0.054 |
| | Benzene | 0.047 ± 0.011 | 0.068 ± 0.009 | 0.066 | 0.066 |
| | iso-Octane | 0.075 ± 0.014 | 0.095 ± 0.010 | 0.094 | 0.091 |
| | n-Dodecane | (*) | (*) | (*) | (*) |
| Stanford A [23] | Methylcyclohexane | 0.036 ± 0.013 | 0.044 ± 0.008 | 0.056 | 0.064 |
| | Toluene | 0.047 ± 0.008 | 0.033 ± 0.006 | 0.057 | 0.057 |
| | Benzene | 0.076 ± 0.010 | 0.092 ± 0.008 | 0.064 | 0.062 |
| | iso-Octane | 0.260 ± 0.016 | 0.301 ± 0.007 | 0.288 | 0.283 |
| | n-Dodecane | (*) | (*) | (*) | (*) |
| Stanford B [23] | Methylcyclohexane | 0.033 ± 0.005 | 0.066 ± 0.006 | 0.055 | 0.078 |
| | Toluene | 0.237 ± 0.007 | 0.255 ± 0.006 | 0.240 | 0.242 |
| | Benzene | 0.084 ± 0.008 | 0.055 ± 0.006 | 0.075 | 0.067 |
| | iso-Octane | 0.084 ± 0.005 | 0.088 ± 0.006 | 0.078 | 0.080 |
| | n-Dodecane | (*) | (*) | (*) | (*) |

Table 7: Summary of hyperellipsoidal characterizations using error thresholds presented in Table 2 with IDT or linear mole-fraction blended DCN for the jet fuel surrogates proposed in [3, 7, 23]. $\mathbf{x}_{AA}$ and $\mathbf{x}_{MV}$ correspond to axis-aligned (AA) and maximum-volume (MV) centers respectively. The last species is obtained from enforcing total species conservation and is denoted by (*)

Tables 6 and 7 summarize the four surrogate mixtures and their characterizations using a linear mole-fraction blended DCN (referred to as "Blended") instead of the ignition delay time as a CPT. The differences are clear as they are present for every surrogate composition and characterization, thus highlighting the importance of using consistent and uniform definitions of CPTs while evaluating surrogate compositions. Some of the mole fractions differ by over 20%, as observed in the case of iso-octane for various JP-8 surrogates. In fact, the range of the feasible region predicted itself is non-overlapping for Stanford A surrogate and further stresses the importance of using a particular model for evaluating the CPT. Once the CPT and its method of evaluation is fixed, the next variable is the error threshold, and its effect on the final surrogate composition is discussed in the next section.

## 4. Multi-parametric optimization approach to surrogate representation

The results presented so far assume that the error thresholds are fixed and it is useful to study the variation of composition ranges with thresholds as it provides a measure of sensitivity. This translates to being able to solve the convex optimization problems presented in Section 2 with the error thresholds as parameters. The theory for multi-parametric optimization is well-developed in the case of linear constraints and objective functions [42] and helps to achieve the same.

Molecular weight, H/C ratio, TSI and sum of mole fractions are the linear constraints in Eq. (4) and can be visualized as planes demarcating feasible regions in composition space. However, when the problem is to be solved with $\epsilon_{HC}$ as a parameter, the H/C constraint can be written as

$$\begin{aligned} (\mathbf{h} - t_{HC}(1-\epsilon_{HC})\mathbf{c})^T\mathbf{x} \geq 0 \\ (\mathbf{h} - t_{HC}(1+\epsilon_{HC})\mathbf{c})^T\mathbf{x} \leq 0 \end{aligned} \tag{9}$$

Equation (9) represents a 'bilinear' constraint due to the product of the parameter $\epsilon_{HC}$ and the optimization variable $\mathbf{x}$, both of which are unknowns in a multi-parametric optimization problem. Such bilinear constraints are, however, computationally tractable and can be solved by relaxing the original optimization problem using McCormick envelopes [43].

The main benefit of the multi-parametric approach is that one can obtain information as functions of the error thresholds, which would have previously taken one complete solution to the optimization problem for each parameter set. To illustrate the use of the multi-parametric approach, the lower and upper bounds for mole fractions are derived for the surrogate mixtures presented in Table 1, as a function of the two linear constraints, molecular weight and TSI. The objective function is identical to the one utilized in constructing the outer hypercuboid. The restriction to only linear constraints is because existing multi-parametric optimization solvers are compatible only with such constraints [44]. The optimization problem

can be summarized as

$$
\begin{aligned}
z(\mathbf{x}, \epsilon_{MW}, \epsilon_{TSI}) := \underset{\mathbf{x}}{\text{minimize/maximize}} \quad & x_i \\
\text{subject to} \quad & \sum_{i=1}^{N_s} x_i = 1 \\
& -\epsilon_{MW} \leq \mathbf{m}^T\mathbf{x} - t_{MW} \leq \epsilon_{MW} \\
& -\epsilon_{TSI} \leq \frac{\mathbf{h}^T\mathbf{x}}{\mathbf{c}^T\mathbf{x}} - t_{TSI} \leq \epsilon_{TSI}
\end{aligned}
\tag{10}
$$

Although the optimal can be expressed in closed form for linear objective functions and constraints, the use of computational tools is necessary to identify the regions of applicability of a particular solution. The optimal solutions are piecewise-linear functions and can be expressed in terms of error thresholds. The multi-parametric optimization was performed using the MPT3 toolbox [44], which was also coupled with Cantera [45] for obtaining other physicochemical properties.

Figure 12 shows the lower and upper bounds of mole fractions as a function of the specified molecular weight and TSI threshold. The proposed experimental compositions lie along the $\epsilon_{MW}, \epsilon_{TSI} = 0$ line as they correspond to the exact target properties. The threshold is depicted up to an arbitrary value of 25 g/mol to specifically illustrate that it can be evaluated beyond the prescribed experimental uncertainty of 6 g/mol in [14]. Similarly, the TSI threshold is presented up to an arbitrary value of 4. Two planes - each corresponding to the lower and upper bound are presented for each compound in the palette. The experimental composition always lies between these planes, thus demonstrating the consistency between experimental and multi-parametric approaches to surrogate representation. The optimal solutions obtained using computations are indeed verified to be piecewise-linear functions of the error thresholds, as expected from the theory of multi-parametric optimization [42, pg. 8].

Once the compositions are known as functions of error thresholds, the problem of determining the effect of a particular constraint simply translates to evaluating the slope of these piecewise-linear functions at the given error thresholds. Thus, knowledge about sensitivity coefficients, optimal weighting factors and dual variables, which are equivalent upto constant factors as discussed in Section 3.2 can be obtained directly. It is important to remember that these depend on the objective function under consideration and should not be used to provide generalizations regarding the constraints or palette compounds.

## 5. Conclusions

In this work, a computational procedure is presented to construct surrogate descriptions of fuels using information on experimental uncertainty. This study also provides a sound theoretical foundation using tools from optimization theory and the described computational procedure is compared with experimental surrogates for two aviation fuels, Jet-A and JP-8. Also, a consistent description of physical properties of fuels

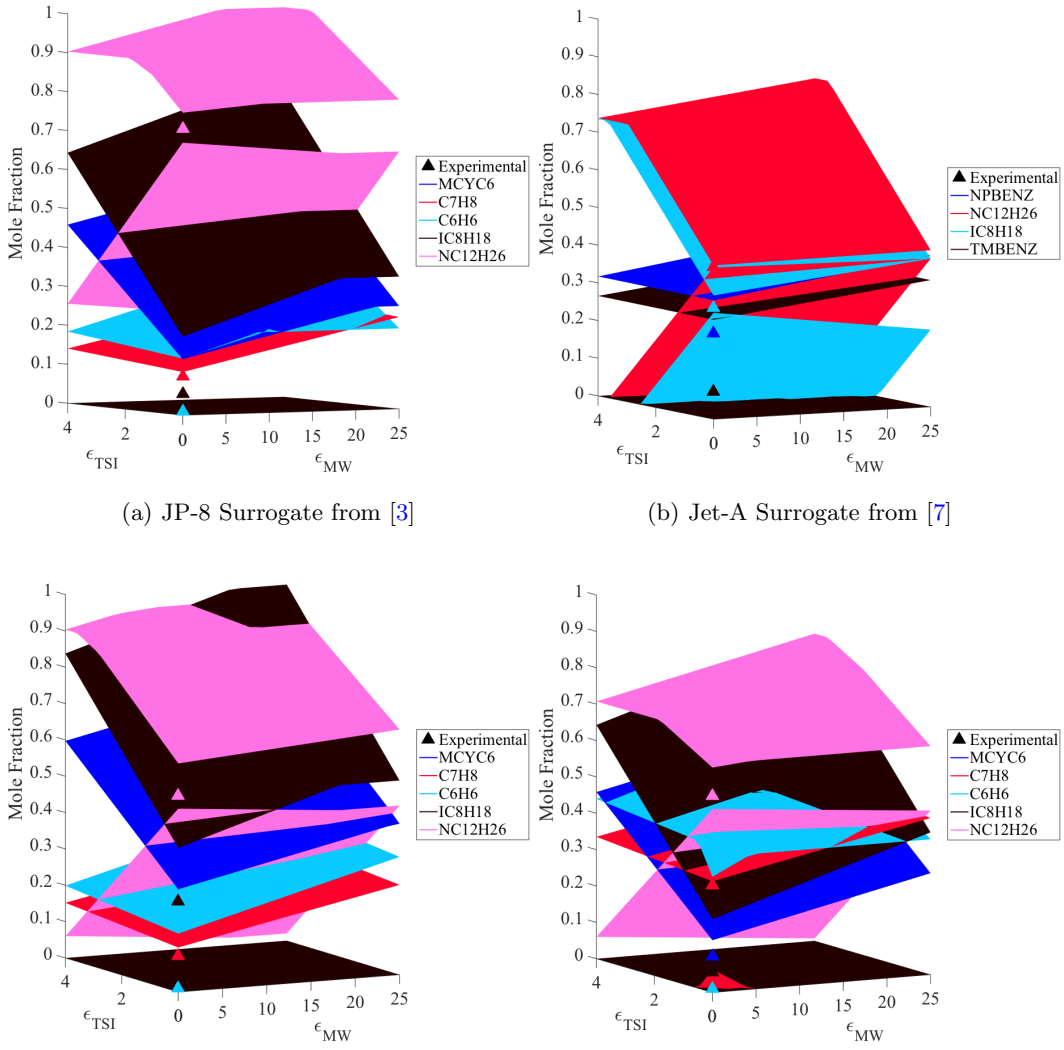


(a) JP-8 Surrogate from [3]

(b) Jet-A Surrogate from [7]

(c) JP-8 Surrogate (Stanford A) from [23]

(d) JP-8 Surrogate (Stanford B) from [23]

Figure 12: Lower and upper bound of mole fractions in surrogates proposed in [3, 7, 23] respectively as a function of the molecular weight threshold $\epsilon_{MW}$, which ranges from $0 \leq \epsilon_{MW} \leq 25$ (g/mol)

in surrogate descriptions is presented through the use of the recent ASTM D2887 standard. Both physical and chemical combustion property targets, including ignition delay time and distillation curve errors, are used for the characterization of surrogates in the presence of experimental uncertainty. Particularly, agreement between experimental and computational descriptions of surrogates is shown to ensure consistency between the two concepts. Most of all, it is shown that surrogate compositions require the description using a feasible region and are thus not unique. Key findings on the importance of particular CPTs and weighting factors in existing computational approaches using the proposed theoretical background are presented. The equivalence of weighting factors, sensitivity coefficients and dual variables is shown under plausible assumptions. The

effect of using simplified models for CPTs on the final surrogate composition is shown using the example of linear blending rules for ignition delay. The framework for multi-parametric optimization approach is presented and it is shown that sensitivity information can be obtained as a function of experimental uncertainty by solving only one optimization problem. The question of whether the palette compounds can be obtained using an algorithm can be addressed by generalizing the current optimization framework to mixed-integer programs and will be discussed in subsequent work.

## 6. Acknowledgements

This work was funded by the US Federal Aviation Administration (FAA) Office of Environment and Energy as part of ASCENT Project National Jet Fuel Combustion Program under FAA Award Number: 13-C-AJFE-SU-010. Financial support through NASA's Transformational Tools and Technologies Program with Award Number: NNX15AV04A is gratefully acknowledged. Any opinions, findings, conclusions or recommendations expressed in this material are those of the authors and do not necessarily reflect the views of the FAA, ASCENT Sponsors, or the U.S. Government. Special thanks to Dr. Tim Edwards of AFRL for providing the ASTM D2887 distillation data on request. We would also like to thank Dr. Tom Bruno at NIST for helpful discussions on distillation measurements. Resources supporting this work were provided by the NASA High-End Computing (HEC) Program through the NASA Advanced Supercomputing (NAS) Division at Ames Research Center.

## Nomenclature

### Greek Symbols

$\beta$ Recovered mass fraction

$\epsilon'_j$ Relative error threshold for $j^{\text{th}}$ CPT

$\epsilon_j$ Absolute error threshold for $j^{\text{th}}$ CPT

$\gamma_j$ Sensitivity coefficient

$\lambda_j$ Dual variable for constraint $j$

$\mathcal{E}$ Ellipsoid

$\theta_i$ Threshold sooting index of compound $i$

### Roman Symbols

$\mathbf{A}$ Polyhedron matrix in composition space

$\mathbf{a}_i$ $i^{th}$ row in constraint matrix

$\mathbf{B}$ Ellipsoid transformation matrix

$\mathbf{b}$ Polyhedron right-hand side in composition space

$\mathbf{l}$ Lower bound of hypercuboid

$\mathbf{m}$ Molecular weight

$\mathbf{Q}$ Ellipsoid quadratic transformation, $\mathbf{Q} = \mathbf{B}\mathbf{B}^T$

$\mathbf{u}$ Upper bound of hypercuboid

$\mathbf{v}$ Constraint perturbation

$\mathbf{w}$ General point in composition space

$\mathbf{x}$ Mole fraction

$c_i$ Number of carbon atoms in species $i$

$d_i$ Derived cetane number of compound i

$f$ Objective function

$F_j$ Constraint function for $j^{\text{th}}$ CPT

$h_i$ Number of hydrogen atoms in species $i$

$N_{nl}$ Number of nonlinear CPTs

$N_s$ Number of species/compounds in palette

$p^*$ Optimal objective when constraints perturbed by $\mathbf{v}$

$p_0$ Ambient pressure

$R$ Chebyshev radius

$S_j$ Feasible region for $j^{\text{th}}$ CPT

$T_0$ Ambient temperature

$t_j$ Target value for $j^{\text{th}}$ CPT

DCN Derived cetane number

**Superscripts**

| | |
|---|---|
| + | Positive entries |
| – | Negative entries |

**Subscripts**

| | |
|---|---|
| AA | Axis-aligned |
| DC | Distillation curve |
| HC | H/C ratio |
| IDT | Ignition delay time |
| in | Inner hypercuboid |
| MV | Maximum-volume |
| MW | Molecular weight |
| TSI | Threshold sooting index |

### Supplementary Information

The MATLAB program to quantify surrogate uncertainty is available online at http://github.com/IhmeGroup/MPT_surr and can be utilized for further characterizations of surrogates. The data for the ignition delay times is generated by a separate parallel Python program, which can also be found online at http://github.com/IhmeGroup/pyIDT.

### A. Numerical methods for surrogate representation

This section discusses the numerical methods used to obtain the surrogate representation in this paper. First, the inner and outer hypercuboids are presented, followed by the discussion on ellipsoids. Despite the similarities in the geometrical idea of using bounding figures, but of different shapes, the discussion in this section clearly illustrates that there are many differences in the numerical approach between hypercuboids and hyperellipsoids. The constraints are approximated using a convex hull, as discussed in Section 2.3 and is thus given by a polyhedron in composition space. This can be concisely represented as $\mathbf{Ax} \leq \mathbf{b}$, where both $\mathbf{A}$ and $\mathbf{b}$ are functions of relative error thresholds $\epsilon_i'$.

*A.1. Hypercuboids*

Suppose $\mathbf{l}$ and $\mathbf{u}$ denote the lower and upper limits of coordinates in composition space of the inner hypercuboid, then $\mathbf{l} \leq \mathbf{x} \leq \mathbf{u}$ denotes the hypercuboid itself. The volume of the hypercuboid is given by $\prod_{i}^{N_s}(u_i - l_i)$. It is necessary to utilize an equivalent objective function which is convex for it to be compatible with optimization solvers [46]. The geometric mean is known to be concave [34, pg. 74] and thus its negative can be minimized while being constrained inside the polytope as a convex optimization problem. It must be ensured that the entire hypercuboid lies inside the polytope and for this, it is sufficient that the vertices satisfy the constraints. However, this leads to an exponential number of constraints and makes the problem computationally intractable. Noting that both $\mathbf{l}$ and $\mathbf{u}$ are non-negative as they represent mole fractions, these constraints are in fact equivalent to a single inequality. Defining $A_{ij}^{+} = \max(0, A_{ij})$ and $A_{ij}^{-} = \min(0, A_{ij})$, the equivalent constraint is given by $\mathbf{A}^{+}\mathbf{u} + \mathbf{A}^{-}\mathbf{l} \leq \mathbf{b}$. In other words, the maximum-volume axis-aligned hypercuboid that strictly lies inside the search space is given by the convex optimization problem

$$\begin{aligned} \underset{\mathbf{x}}{\text{minimize}} \quad & -\text{ geometric mean}(\mathbf{u} - \mathbf{l}) \\ \text{subject to} \quad & \mathbf{A}^{+}\mathbf{u} + \mathbf{A}^{-}\mathbf{l} \leq \mathbf{b} \end{aligned} \tag{11}$$

The outer hypercuboid is easier to construct and essentially involves solving multiple convex optimization problems, each one either minimizing or maximizing a particular coordinate while being restricted to the polytope. This can be written as

$$\begin{aligned} \underset{\mathbf{x}}{\text{minimize/maximize}} \quad & x_i \\ \text{subject to} \quad & \mathbf{A}\mathbf{x} \leq \mathbf{b} \end{aligned} \tag{12}$$

Here, $x_i$ denotes the $i$-th coordinate in composition space.

*A.2. Hyperellipsoids*

As discussed in Section 2.3.2, a hyperellipsoid around the surrogate composition is represented as

$$\mathcal{E} = \{\mathbf{B}\mathbf{w} + \mathbf{x} \text{ such that } \|\mathbf{w}\|_2 \leq 1\} \tag{13}$$

where $\mathbf{B}$ can be assumed, without loss of generality, to be a positive-definite matrix. It is useful to note that axis-aligned hyperellipsoids are given by diagonal matrices. The volume is proportional to the determinant, denoted by $\det(\mathbf{B})$, and its logarithm is commonly used as an objective function, as it can be shown to be a concave function [34, pg. 74]. The search space polytope can be represented plane-wise as $S = \{w \text{ such that } \mathbf{a}_i^T\mathbf{w} \leq b_i\}$. Since the maximum-volume hyperellipsoid must lie completely within this region, it must be that $\sup_{\|w\|_2 \leq 1} \mathbf{a}_i^T(\mathbf{B}\mathbf{w} + \mathbf{x}) \leq b_i$. On expanding the product, it is noted that this is equivalent to

$\|\mathbf{B}\mathbf{a}_i\|_2 + \mathbf{a}_i^T\mathbf{x} \leq b_i$ and serves as the constraint for the optimization problem. With this, the maximal-volume hyperellipsoid can be written as

$$\begin{aligned} \underset{\mathbf{x}}{\text{minimize}} \quad & -\log\det(\mathbf{B}) \\ \text{subject to} \quad & \|\mathbf{B}\mathbf{a}_i\|_2 + \mathbf{a}_i^T\mathbf{x} \leq b_i \end{aligned} \tag{14}$$

Axis-aligned hyperellipsoids cannot be obtained using the previous approach as a diagonal-only constraint on the matrix $\mathbf{B}$ is not a part of disciplined convex programming. However, they can be obtained by fitting a maximal-volume hypersphere in a scaled search space, where it spans equally in all dimensions, and is then rescaled back to the original [47]. The center of the maximum-volume hypersphere is commonly referred to as the *Chebyshev* center and similar terminology is used for the radius and the hypersphere/ball itself. Once again, writing the convex polytope in a plane-wise fashion, it must be that $\sup_{\|u\|_2 \leq 1} \mathbf{a}_i^T(\mathbf{x} + R\mathbf{u}) \leq b_i$ which can be simplified as $\mathbf{a}_i^T\mathbf{x} + R\|\mathbf{a}_i\|_2 \leq b_i$. Thus, the Chebyshev center and radius $R$ can be found by solving the linear program

$$\begin{aligned} \underset{\mathbf{x}}{\text{maximize}} \quad & R \\ \text{subject to} \quad & \mathbf{a}_i^T\mathbf{x} + R\|\mathbf{a}_i\|_2 \leq b_i \\ & R \geq 0 \end{aligned} \tag{15}$$

Once the radius and center are obtained, the space is rescaled back to the original and it is important to remember that both the axes lengths and origin are to be updated. As mentioned in Section 2.3.2, the same approach can be used to fit an arbitrary object inside a polyhedron.

## B. Verification of computational surrogates

This section summarizes the various computational surrogate compositions and verifies that their CPTs are indeed within the prescribed experimental uncertainties. As discussed in Section 3.1, the centers of the inner hypercuboid, axis-aligned hyperellipsoid and maximum-volume hyperellipsoid serve as sample points inside the geometric objects used to describe the feasible region and should satisfy the CPTs within experimental uncertainty. The centers corresponding to each surrogate listed in Table 1 were presented in Tables 3 and 4, and can be summarized for the three geometrical objects under consideration in Tables 8 to 10.

| Name | Methylcyclo-hexane | Tolu-ene | Ben-zene | iso-Octane | n-Dode-cane | n-Propylben-zene | 1,3,5-Trimethyl-benzene |
|---|---|---|---|---|---|---|---|
| Jet-A POSF 4658 (Dooley et al. [7]) | | | | 0.296 | 0.401 | 0.236 | 0.067 |
| JP-8 (Violi et al. [3]) | 0.047 | 0.040 | 0.082 | 0.090 | 0.741 | | |
| JP-8 (Stanford A [23]) | 0.041 | 0.056 | 0.068 | 0.293 | 0.542 | | |
| JP-8 (Stanford B [23]) | 0.056 | 0.265 | 0.050 | 0.083 | 0.546 | | |

Table 8: Compounds used in palettes along with their mole fractions for the inner hypercuboid center $\mathbf{x}_{in}$

| Name | Methylcyclo-hexane | Tolu-ene | Ben-zene | iso-Octane | n-Dode-cane | n-Propylben-zene | 1,3,5-Trimethyl-benzene |
|---|---|---|---|---|---|---|---|
| Jet-A POSF 4658 (Dooley et al. [7]) | | | | 0.296 | 0.397 | 0.236 | 0.071 |
| JP-8 (Violi et al. [3]) | 0.067 | 0.070 | 0.047 | 0.075 | 0.741 | | |
| JP-8 (Stanford A [23]) | 0.036 | 0.047 | 0.076 | 0.260 | 0.581 | | |
| JP-8 (Stanford B [23]) | 0.033 | 0.237 | 0.084 | 0.084 | 0.562 | | |

Table 9: Compounds used in palettes along with their mole fractions for the axis-aligned hyperellipsoid center $\mathbf{x}_{AA}$

| Name | Methylcyclo-hexane | Tolu-ene | Ben-zene | iso-Octane | n-Dode-cane | n-Propylben-zene | 1,3,5-Trimethylben-zene |
|---|---|---|---|---|---|---|---|
| Jet-A POSF 4658 (Dooley et al. [7]) | | | | 0.297 | 0.400 | 0.234 | 0.069 |
| JP-8 (Violi et al. [3]) | 0.05 | 0.055 | 0.066 | 0.094 | 0.735 | | |
| JP-8 (Stanford A [23]) | 0.056 | 0.057 | 0.064 | 0.288 | 0.535 | | |
| JP-8 (Stanford B [23]) | 0.033 | 0.237 | 0.084 | 0.084 | 0.562 | | |

Table 10: Compounds used in palettes along with their mole fractions for the maximum-volume hyperellipsoid center $\mathbf{x}_{MV}$

The CPTs for each surrogate are evaluated at the three centers and are compared with the lower and upper bounds. The results are summarized in Tables 11 to 14.

| CPT | $\mathbf{x}_{in}$ | $\mathbf{x}_{AA}$ | $\mathbf{x}_{MV}$ | Lower Bound | Upper Bound |
|---|---|---|---|---|---|
| Molecular Weight | 138.53 | 138.35 | 138.49 | 131.76 | 145.63 |
| H/C Ratio | 1.957 | 1.954 | 1.958 | 1.950 | 1.969 |
| Threshold Sooting Index | 21.432 | 21.634 | 21.429 | 20.586 | 22.301 |
| Ignition Delay (s) | 14.32e-04 | 14.39e-04 | 14.11e-04 | 12.62e-04 | 16.40e-04 |
| Distillation Curve Error (K) | 52.355 | 52.313 | 52.069 | 51.701 | 53.010 |

Table 11: CPTs evaluated at the inner hypercuboid center ($\mathbf{x}_{in}$), axis-aligned hyperellipsoid ($\mathbf{x}_{AA}$) and maximum-volume hyperellipsoid ($\mathbf{x}_{MV}$) along with lower and upper bounds based on the experimental uncertainties in Table 2 for the Jet-A surrogate in [2]

| CPT | $\mathbf{x}_{in}$ | $\mathbf{x}_{AA}$ | $\mathbf{x}_{MV}$ | Lower Bound | Upper Bound |
|---|---|---|---|---|---|
| Molecular Weight | 151.00 | 151.33 | 150.63 | 143.73 | 158.86 |
| H/C Ratio | 2.085 | 2.086 | 2.085 | 2.069 | 2.094 |
| Threshold Sooting Index | 9.768 | 9.852 | 9.839 | 9.447 | 10.234 |
| Ignition Delay (s) | 5.99e-04 | 6.09e-04 | 6.18e-04 | 5.15e-04 | 6.29e-04 |
| Distillation Curve Error (K) | 94.400 | 94.703 | 94.541 | 93.699 | 96.071 |

Table 12: CPTs evaluated at the inner hypercuboid center ($\mathbf{x}_{in}$), axis-aligned hyperellipsoid ($\mathbf{x}_{AA}$) and maximum-volume hyperellipsoid ($\mathbf{x}_{MV}$) along with lower and upper bounds based on the experimental uncertainties in Table 2 for the JP-8 surrogate in [3]

| CPT | $\mathbf{x}_{in}$ | $\mathbf{x}_{AA}$ | $\mathbf{x}_{MV}$ | Lower Bound | Upper Bound |
|---|---|---|---|---|---|
| Molecular Weight | 139.20 | 141.91 | 139.61 | 133.28 | 147.31 |
| H/C Ratio | 2.092 | 2.092 | 2.092 | 2.079 | 2.100 |
| Threshold Sooting Index | 9.719 | 9.780 | 9.804 | 9.409 | 10.194 |
| Ignition Delay (s) | 8.26e-04 | 7.78e-04 | 8.48e-04 | 7.46e-04 | 9.17e-04 |
| Distillation Curve Error (K) | 96.037 | 95.431 | 95.875 | 95.175 | 97.585 |

Table 13: CPTs evaluated at the inner hypercuboid center ($\mathbf{x}_{in}$), axis-aligned hyperellipsoid ($\mathbf{x}_{AA}$) and maximum-volume hyperellipsoid ($\mathbf{x}_{MV}$) along with lower and upper bounds based on the experimental uncertainties in Table 2 for the JP-8 Stanford A surrogate presented in [23]

It can be observed that every CPT for all centers and surrogates lie within the range of experimental uncertainty, and thus within the feasible region. Thus, the surrogates obtained from computations are consistent with experimental descriptions up to the reported range of uncertainties and hence, unifying both

| CPT | $\mathbf{x}_{in}$ | $\mathbf{x}_{AA}$ | $\mathbf{x}_{MV}$ | Lower Bound | Upper Bound |
|---|---|---|---|---|---|
| Molecular Weight | 136.19 | 136.81 | 136.15 | 129.20 | 142.80 |
| H/C Ratio | 1.934 | 1.934 | 1.935 | 1.902 | 1.939 |
| Threshold Sooting Index | 15.624 | 15.583 | 15.429 | 14.902 | 16.144 |
| Ignition Delay (s) | 7.67e-04 | 7.72e-04 | 7.68e-04 | 7.07e-04 | 8.92e-04 |
| Distillation Curve Error (K) | 97.148 | 96.986 | 96.946 | 96.931 | 99.385 |

Table 14: CPTs evaluated at the inner hypercuboid center ($\mathbf{x}_{in}$), axis-aligned hyperellipsoid ($\mathbf{x}_{AA}$) and maximum-volume hyperellipsoid ($\mathbf{x}_{MV}$) along with lower and upper bounds based on the experimental uncertainties in Table 2 for the JP-8 Stanford B surrogate presented in [23]

computational and experimental surrogate descriptions.

## References


[1] T. J. Edwards, L. Q. Maurice, Surrogate mixtures to represent complex aviation and rocket fuels, Journal of Propulsion and Power 17 (2) (2001) 461–466.

[2] S. Dooley, S. H. Won, M. Chaos, J. Heyne, Y. Ju, F. L. Dryer, K. Kumar, C.-J. Sung, H. Wang, M. A. Oehlschlaeger, et al., A jet fuel surrogate formulated by real fuel properties, Combustion and Flame 157 (12) (2010) 2333–2339.

[3] A. Violi, S. Yan, E. Eddings, A. Sarofim, S. Granata, T. Faravelli, E. Ranzi, Experimental formulation and kinetic model for JP-8 surrogate mixtures, Combustion Science and Technology 174 (11-12) (2002) 399–417.

[4] P. Dagaut, A. El Bakali, A. Ristori, The combustion of kerosene: Experimental results and kinetic modelling using 1-to 3-component surrogate model fuels, Fuel 85 (7) (2006) 944–956.

[5] W. J. Pitz, N. P. Cernansky, F. L. Dryer, F. N. Egolfopoulos, J. T. Farrell, D. G. Friend, H. Pitsch, Development of an experimental database and chemical kinetic models for surrogate gasoline fuels, SAE Technical Paper (2007) 01–0175.

[6] W. J. Pitz, C. J. Mueller, Recent progress in the development of diesel surrogate fuels, Progress in Energy and Combustion Science 37 (3) (2011) 330–350.

[7] S. Dooley, S. H. Won, J. Heyne, T. I. Farouk, Y. Ju, F. L. Dryer, K. Kumar, X. Hui, C.-J. Sung, H. Wang, et al., The experimental evaluation of a methodology for surrogate fuel formulation to emulate gas phase combustion kinetic phenomena, Combustion and Flame 159 (4) (2012) 1444–1466.

[8] M. Colket, T. J. Edwards, N. P. Cernansky, F. L. Dryer, F. Egolfopoulos, D. Friend, C. K. Law, D. Lenhert, P. L. Lindstedt, H. Pitsch, et al., Development of an experimental database and kinetic models for surrogate jet fuels, in: 45th AIAA Aerospace Sciences Meeting and Exhibit, AIAA Paper 2007-770, 2007.

[9] K. V. Puduppakkam, L. Liang, C. V. Naik, E. Meeks, B. G. Bunting, Combustion and emissions modeling of a gasoline HCCI engine using model fuels, SAE Technical Paper (2009) 01–0669.

[10] C. J. Mueller, W. J. Cannella, T. J. Bruno, B. Bunting, H. D. Dettman, J. A. Franz, M. L. Huber, M. Natarajan, W. J. Pitz, M. A. Ratcliff, et al., Methodology for formulating diesel surrogate fuels with accurate compositional, ignition-quality, and volatility characteristics, Energy & Fuels 26 (6) (2012) 3284–3303.

[11] A. Ahmed, G. Goteng, V. S. Shankar, K. Al-Qurashi, W. L. Roberts, S. M. Sarathy, A computational methodology for formulating gasoline surrogate fuels with accurate physical and chemical kinetic properties, Fuel 143 (2015) 290–300.

[12] D. Kim, J. Martz, A. Violi, A surrogate for emulating the physical and chemical properties of conventional jet fuel, Combustion and Flame 161 (6) (2014) 1489–1498.

[13] D. Kim, J. Martz, A. Abdul-Nour, X. Yu, M. Jansons, A. Violi, A six-component surrogate for emulating the physical and chemical characteristics of conventional and alternative jet fuels and their blends, Combustion and Flame 179 (2017) 86–94.

[14] S. H. Won, F. M. Haas, S. Dooley, T. J. Edwards, F. L. Dryer, Reconstruction of chemical structure of real fuel by surrogate formulation based upon combustion property targets, Combustion and Flame 183 (2017) 39–49.

[15] Y. Ra, R. D. Reitz, A vaporization model for discrete multi-component fuel sprays, International Journal of Multiphase Flow 35 (2) (2009) 101–117.

[16] A. Elwardany, S. S. Sazhin, A. Farooq, Modelling of heating and evaporation of gasoline fuel droplets: A comparative analysis of approximations, Fuel 111 (2013) 643–647.

[17] T. J. Bruno, L. S. Ott, T. M. Lovestead, M. L. Huber, Relating complex fluid composition and thermophysical properties with the advanced distillation curve approach, Chemical Engineering & Technology 33 (3) (2010) 363–376.

[18] T. J. Bruno, B. L. Smith, Evaluation of the physicochemical authenticity of aviation kerosene surrogate mixtures. Part 1: Analysis of volatility with the advanced distillation curve, Energy & Fuels 24 (8) (2010) 4266–4276.

[19] T. J. Bruno, M. L. Huber, Evaluation of the physicochemical authenticity of aviation kerosene surrogate mixtures. Part 2: Analysis and prediction of thermophysical properties, Energy & Fuels 24 (8) (2010) 4277–4284.

[20] ASTM D86, Standard Test Method for Distillation of Petroleum Products at Atmospheric Pressure, ASTM International.

[21] T. J. Bruno, B. L. Smith, Improvements in the measurement of distillation curves. 2. Application to aerospace/aviation fuels RP-1 and S-8, Industrial & Engineering Chemistry Research 45 (12) (2006) 4381–4388.

[22] ASTM D2887, Standard test method for boiling range distribution of petroleum fractions by gas chromatography, ASTM International, Vol. 05.01 (2008).

[23] S. S. Vasu, D. F. Davidson, R. K. Hanson, Jet fuel ignition delay times: Shock tube experiments over wide conditions and surrogate model predictions, Combustion and Flame 152 (1) (2008) 125–143.

[24] E. Ranzi, A. Frassoldati, R. Grana, A. Cuoci, T. Faravelli, A. Kelley, C. K. Law, Hierarchical and comparative kinetic modeling of laminar flame speeds of hydrocarbon and oxygenated fuels, Progress in Energy and Combustion Science 38 (4) (2012) 468–501.

[25] P. B. Govindaraju, M. Ihme, Group contribution method for multicomponent evaporation with application to transportation fuels, International Journal of Heat and Mass Transfer 102 (2016) 833–845.

[26] E. Ranzi, A wide-range kinetic modeling study of oxidation and combustion of transportation fuels and surrogate mixtures, Energy & Fuels 20 (3) (2006) 1024–1032.

[27] P. Pepiot-Desjardins, H. Pitsch, R. Malhotra, S. Kirby, A. Boehman, Structural group analysis for soot reduction tendency of oxygenated fuels, Combustion and Flame 154 (1) (2008) 191–205.

[28] L. N. Allard, G. D. Webster, N. J. Hole, T. W. Ryan, D. Ott, C. W. Fairbridge, Diesel fuel ignition quality as determined in the ignition quality tester (IQT), SAE Technical Paper (1996) 961182.

[29] A. Frassoldati, A. Cuoci, T. Faravelli, U. Niemann, E. Ranzi, R. Seiser, K. Seshadri, An experimental and kinetic modeling study of n-propanol and iso-propanol combustion, Combustion and Flame 157 (1) (2010) 2–16.

[30] D. F. Davidson, M. A. Oehlschlaeger, J. T. Herbon, R. K. Hanson, Shock tube measurements of iso-octane ignition times and oh concentration time histories, Proceedings of the Combustion Institute 29 (1) (2002) 1295–1301.

[31] T. J. Bruno, L. S. Ott, B. L. Smith, T. M. Lovestead, Complex fluid analysis with the advanced distillation curve approach, Analytical Chemistry 82(3) (2010) 777–783.

[32] M. L. Huber, B. L. Smith, L. S. Ott, T. J. Bruno, Surrogate mixture model for the thermophysical properties of synthetic aviation fuel S-8: Explicit application of the advanced distillation curve, Energy & Fuels 22 (2) (2008) 1104–1114.

[33] T. Edwards, Reference jet fuels for combustion testing, in: 55th AIAA Aerospace Sciences Meeting, 2017-0146.

[34] S. Boyd, L. Vandenberghe, Convex Optimization, Cambridge University Press, 2004.

[35] J. F. Sturm, Using SeDuMi 1.02, a MATLAB toolbox for optimization over symmetric cones, Optimization Methods and Software 11 (1-4) (1999) 625–653.

[36] R. H. Tütüncü, K.-C. Toh, M. J. Todd, Solving semidefinite-quadratic-linear programs using SDPT3, Mathematical Programming 95 (2) (2003) 189–217.

[37] R. Horst, H. Tuy, Global Optimization: Deterministic Approaches, Springer Science & Business Media, 2013.

[38] A. A. Kurzhanskiy, P. Varaiya, Ellipsoidal toolbox (ET), in: Decision and Control, 2006 45th IEEE Conference on, IEEE, 2006, pp. 1498–1503.

[39] D. W. Peterson, A review of constraint qualifications in finite-dimensional spaces, SIAM Review 15 (3) (1973) 639–654.

[40] N. Pasadakis, V. Gaganis, C. Foteinopoulos, Octane number prediction for gasoline blends, Fuel Processing Technology 87 (6) (2006) 505–509.

[41] M. J. Murphy, J. D. Taylor, R. L. McCormick, Compendium of experimental cetane number data, National Renewable Energy Laboratory Golden, CO, 2004.

[42] E. Pistikopoulos, A. Galindo, V. Dua, E. S. Kikkinides, L. Papageorgiou, W. Jorisch, K.-W. Benz, W. Neumann, M. Köhler, W. Fritzsche, et al., Multi-Parametric Programming: Theory, Algorithms and Applications, Wiley, 2007.

[43] G. P. McCormick, Computability of global solutions to factorable nonconvex programs: Part I—Convex underestimating problems, Mathematical Programming 10 (1) (1976) 147–175.

[44] M. Kvasnica, P. Grieder, M. Baotić, M. Morari, Multi-parametric toolbox (MPT), in: International Workshop on Hybrid Systems: Computation and Control, Springer, 2004, pp. 448–462.

[45] D. G. Goodwin, H. K. Moffat, R. L. Speth, Cantera: An Object-oriented Software Toolkit for Chemical Kinetics, Thermodynamics, and Transport Processes, http://www.cantera.org, Version 2.3.0 (2017).

[46] M. Grant, S. Boyd, CVX: MATLAB Software for Disciplined Convex Programming, http://cvxr.com/cvx, Version 2.1 (2014).

[47] S. Director, G. Hachtel, The simplicial approximation approach to design centering, IEEE Transactions on Circuits and Systems 24 (7) (1977) 363–372.